A Volcano Rekindled: The Renewed Eruption of Mount St. Helens, 2004–2006
Edited by David R. Sherrod, William E. Scott, and Peter H. Stauffer
U.S. Geological Survey Professional Paper 1750, 2008

Chapter 8

Use of Digital Aerophotogrammetry to Determine Rates of Lava Dome Growth, Mount St. Helens, Washington, 2004–2005

By Steve P. Schilling[1], Ren A. Thompson[2], James A. Messerich[2], and Eugene Y. Iwatsubo[1]

Abstract

Beginning in October 2004, a new lava dome grew on the glacier-covered crater floor of Mount St. Helens, Washington, immediately south of the 1980s lava dome. Seventeen digital elevation models (DEMs) constructed from vertical aerial photographs have provided quantitative estimates of extruded lava volumes and total volume change. To extract volumetric changes and calculate volumetric extrusion rates (magma discharge rates), each DEM surface was compared to preeruption DEM reference surfaces from 1986 and 2003. Early in the 2004–5 eruption, DEMs documented deforming glacier ice and crater floor that formed a prominent "welt" having a volume of 10×10^6 m^3 and a growth rate of 8.9 m^3/s before dacite lava first appeared at the surface on October 11, 2004. Afterward, the rate was initially 5.9 m^3/s but slowed to 2.5 m^3/s by the beginning of January 2005. During 2005, the extrusion rate declined gradually to about 0.7 m^3/s. By December 15, 2005, the new dome complex was about 900 m long and 625 m wide and reached 190 m above the 2003 surface. More than 73×10^6 m^3 of dacite lava had extruded onto the crater floor.

Successful application of aerophotogrammetry was possible during the critical earliest parts of the eruption because we had baseline data and photogrammetric infrastructure in place before the eruption began. The vertical aerial photographs, including the DEMs and calculations derived from them, were one of the most widely used data sets collected during the 2004–5 eruption, as evidenced in numerous contributions to this volume. These data were used to construct photogeologic maps, deformation vector fields, and profiles of the evolving dome and glacier. Extruded volumes and rates proved to be critical parameters to constrain models and hypotheses of eruption dynamics and thus helped to assess volcano hazards.

Introduction

The volume of a growing lava dome and its extrusion rate are primary measurements that may be compared with other traditional volcano-monitoring data from ground deformation, gas geochemistry, and seismicity for the purpose of monitoring and studying erupting volcanoes. Such comparisons have been made for some recent dome-building eruptions, including Santiaguito, Guatemala (Harris and others, 2003); Unzen, Japan (Nakada and others, 1999); Redoubt, Alaska (Miller, 1994); and Soufrière Hills, Montserrat (Sparks and others, 1998). In addition to their value as a fundamental dataset, volumetric data are needed to explore such linkages as extrusion rate thresholds for transition to explosive activity and volume thresholds for initiation of large-scale dome collapse. In this paper, we describe a new application of traditional photogrammetric techniques to track the growth of the 2004–5 Mount St. Helens lava dome.

In October 2004, a new period of dome growth began at Mount St. Helens that changed the topography of the 1980 crater dramatically (fig. 1). Between October 2004 and December 2005, more than 73×10^6 m^3 of solid dacite lava extruded onto the crater floor immediately south of the lava dome that had formed in the 1980s. The new dome grew as a succession of large spines (Vallance and others, this volume, chap. 9). Dome growth intensely deformed and divided Crater Glacier, which had developed from a small debris-covered snowbank in 1985 into a glacier covering about 1 km^2 by 2001 (Schilling and others, 2004). We use the informal names "west

[1] U.S. Geological Survey, 1300 SE Cardinal Court, Vancouver, WA 98683

[2] U.S. Geological Survey, Box 25046, Denver Federal Center, Denver, CO 80225

Crater Glacier" and "east Crater Glacier" for the two ice bodies remaining within the crater. The growing dome compressed the east Crater Glacier against the east crater wall, resulting in spectacular thickening. Compression and thickening created crevasses and rapid advance of the terminus, about 185 m in two years, followed by similar effects on the west Crater Glacier (Walder and others, this volume, chap. 13).

The extruded volume and extrusion rate of lava associated with this protracted dome eruption are critical parameters used to constrain models of the magmatic system (Mastin and others, this volume, chap. 22) and eruption dynamics (Iverson, this volume, chap. 21), to determine how the magmatic system relates to surface measurements of magmatic gases (Gerlach and others, this volume, chap. 26) and seismicity (for example, to determine if extrusion rate correlates with size and rate of occurrence of volcano-related earthquakes; Moran and others, this volume, chap. 2), and to constrain calculations that address loading effects of the growing dome on surface deformation (Lisowski and others, this volume, chap. 15).

Photogrammetry based on vertical aerial photographs has been used previously to monitor, model, map, and measure surface change and deformation at volcanoes (Achilli and others, 1998; Baldi and others, 2000, 2005; Zlotnicki and others, 1990). A recent photogrammetric study of the Mount St. Helens crater (Schilling and others, 2004) tied a block of overlapping vertical aerial photographs to a network of global positioning system (GPS) stations on the volcano's flanks, dome, and crater floor (fig. 2*A*) resulting in a digital elevation model (DEM) of the volcanic edifice and entire crater configuration in October 2000.

The 2000 DEM has served as a baseline for comparison with past DEMs. Comparison of the 2000 surface with post-May 18, 1980, and 1990 DEMs, both derived from existing topographic contour maps, produced volume estimates of

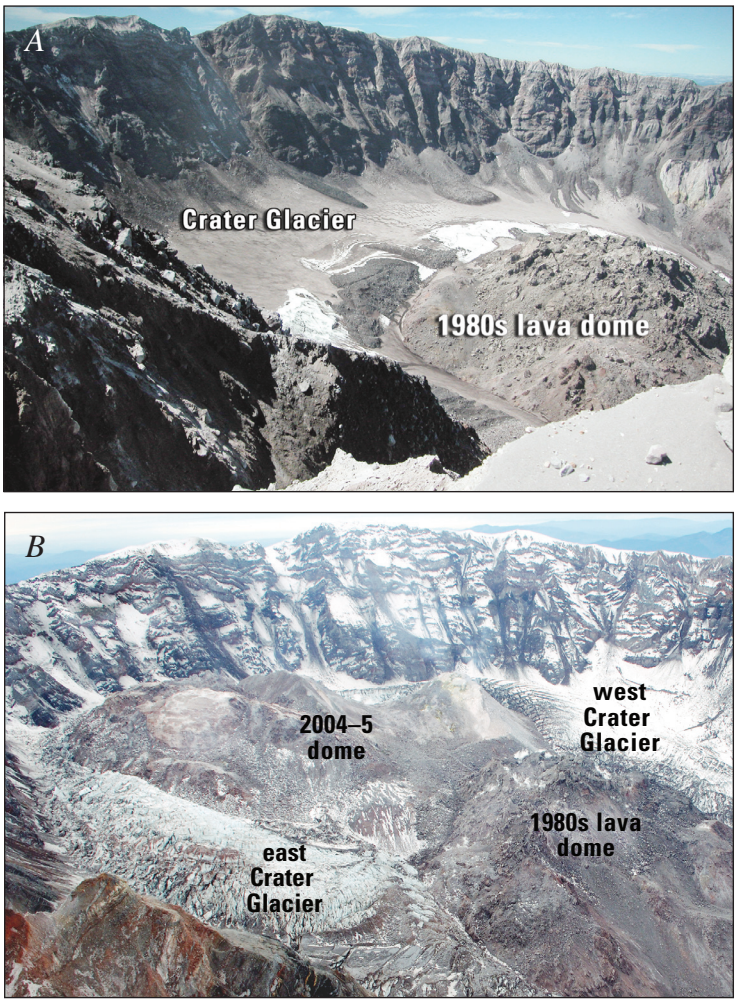

Figure 1. Oblique photographs of Mount St. Helens crater from east rim; views to southwest. *A*, Preeruption crater on August 30, 2004, showing 1980s lava dome and Crater Glacier (mostly coated with rock debris). *B*, Crater on October 12, 2005, showing new lava dome dividing and deforming glacier. USGS photographs by S.P. Schilling.

glacier ice and talus accumulation, as well as crater-wall erosion (Thompson and Schilling, 2007). Near the beginning of the 2004–5 eruption, two other craterwide DEMs were constructed to estimate volume change. One was created from digital, photogrammetrically derived contours that depicted the crater in November 1986, and another was constructed from lidar data (Queija and others, 2005) obtained September 20–22, 2003, using the same network of GPS sites for ground control that was used for photogrammetric monitoring.

Throughout the 2004–5 eruption, we used analytical photogrammetry and a softcopy (that is, digital image) system to provide stereo imaging and accurate measurement of the rapidly changing crater morphology. Seventeen DEMs have been constructed from vertical aerial photographs (Messerich and others, 2008), collected approximately every three weeks, in order to quantify volumetric changes associated with dome growth and collapse as well as deformation of Crater Glacier (Walder and others, this volume, chap. 13). Each new DEM was compared to preeruption reference surfaces of the crater in 1986 and 2003 to extract volumetric changes. For viewing purposes, each DEM was also converted to a hillshade-relief map, in the form of digital raster images (tagged image file format) and corresponding georeferenced world files (ASCII format). These raster maps are found in appendix 1, which is available in the DVD that accompanies this volume and in online versions of this chapter.

Methods

Acquiring low-altitude aerial photographs in inclement weather over mountainous terrain presents logistical challenges, and taking them over an erupting composite volcano such as Mount St. Helens, where rapid turnaround of data is needed to evaluate hazards, adds urgency. These problems were simplified by taking advantage of photogrammetric infrastructure set up during previous work at the volcano (Schilling and others, 2004). When the 2004–5 eruption began, however, some established flight-planning procedures required modification, such as selection of new ground control sites and design of flight lines for appropriate photograph scale

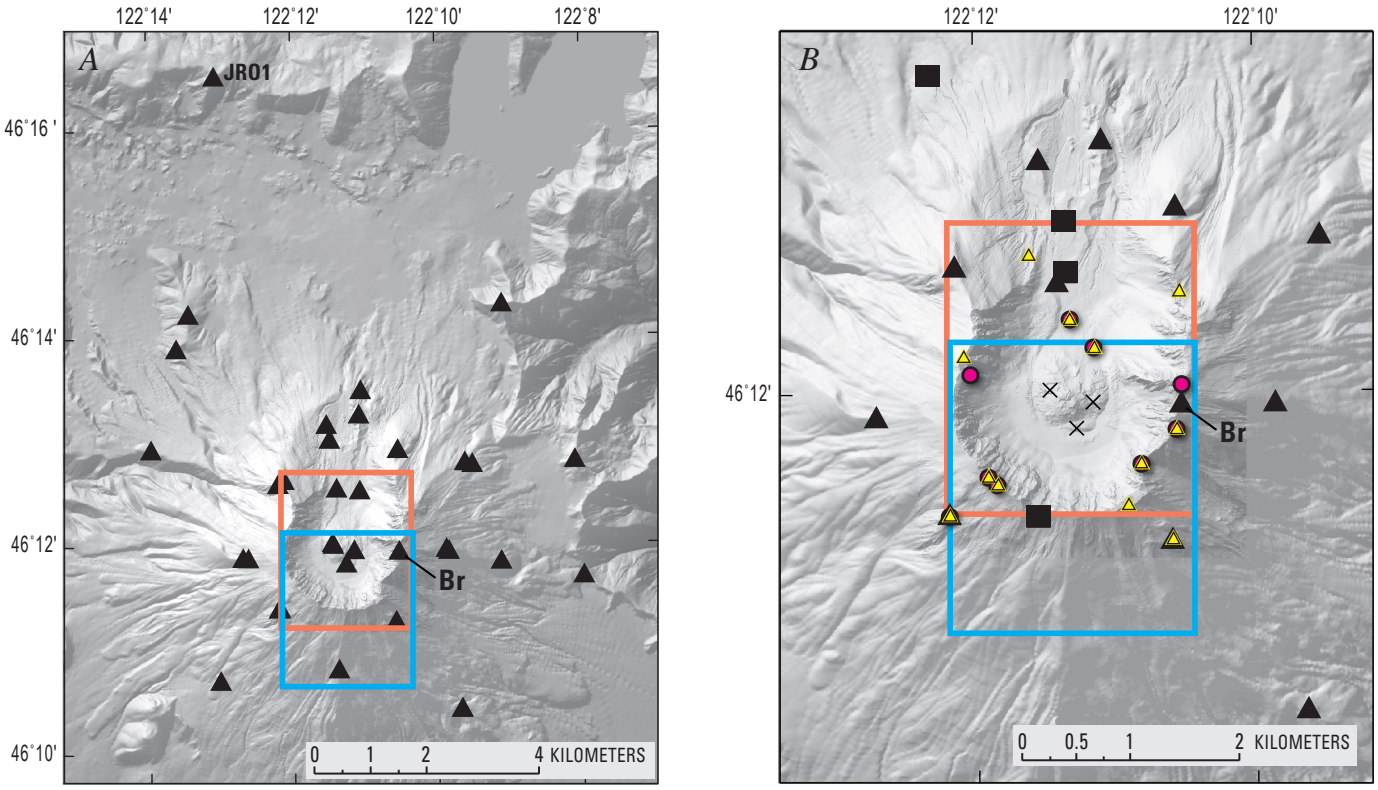

Figure 2. Shaded-relief maps of preeruption surface of Mount St. Helens (2003 DEM). Red and blue boxes show approximate areas covered by two overlapping, 1:12,000-scale vertical aerial photographs. *A*, Broad GPS ground control network (black triangles) used for aerotriangulation of block of photographs to extract coordinates for construction of 2000 DEM and to serve as control for 2003 lidar-based DEM. Br, Brutus control point on east rim. *B*, Ground control points for vertical aerial photographs obtained during 2004–5 eruption. Black X's, ground control points destroyed early in eruption. Red dots, photoidentified control points transferred from 2000 aerotriangulation for use early in eruption. Black squares, new, and black triangles, existing ground control points measured in summer 2005. Yellow triangles, photoidentified control points transferred from August 2005 aerotriangulation solution to serve as ground control for December 2005 aerotriangulation.

and overlap. Early in the eruption, having procedures already established meant that DEMs were constructed rapidly, at times within a few days of obtaining the aerial photographs.

Digital photogrammetry refers to photogrammetric systems that have been adapted from hardcopy (film) aerial photographs mounted on optical-mechanical stereo plotters to softcopy (scanned, digital) aerial photographs imported into a desktop computer workstation. Hardware for our softcopy system includes a fast central processing unit, abundant memory, two display screens (one for stereo images and one for control menus), polarizing spectacles for viewing onscreen images in stereo, and a customized mouse to control three-dimensional (3D) cursor movement. Socet Set software includes spatial resection and spatial intersection algorithms to calculate X, Y, and Z ground coordinates of features observed in stereo aerial photographs; it requires precise camera calibration parameters, carefully measured photograph coordinates, and accurate GPS ground control (Wolf and Dewitt, 2000; Thompson and Schilling, 2007). The softcopy system automates many standard photogrammetric tasks, such as inner and relative orientations of stereo models. However, the critical task of exterior orientation, which ties photographs to ground control, requires a skilled operator to maintain precision. Assuming minimal operator error, the accuracy of the final model solution is constrained by flight height, which determines scale, and by scanning resolution, which determines the minimum feature size that the operator can discern in the aerial photographs.

After considering many factors, such as safety and size of features to be measured, we selected a flying height of 3,900 m (12,800 ft), yielding a nominal photo scale of 1:12,000 with a 153.681-mm lens and 9×9-inch film format. Thus, 1 mm on the photograph at nominal scale represents 12 m on the ground. This nominal scale applies at about the altitude of the Crater Glacier surface immediately south of the 1980s lava dome, roughly midway through the range of relief within the Mount St. Helens crater—from about 2,540 m (8,330 ft) on the crater rim to about 1,815 m (5,955 ft) near the base of the 1980s dome. The variation in altitude corresponds to a variation in scale, often within a single photograph, from 1:8,964 at the rim to 1:13,726 at the base of the 1980s lava dome.

Each aerial photographic negative was scanned at 12 μm resolution, generating a graytone digital image roughly 350 megabytes in size. Owing to the scale variation within a photograph, each cell in the image may represent a different distance on the ground, from 0.108 to 0.165 m.

Global Positioning System (GPS) Control Network

Accurate ground control is equally as important as high-resolution scanning. About 30 GPS sites on the outer flanks, 1980s lava dome, and crater floor of Mount St. Helens (fig. 2*A*) form a network of ground control points for photogrammetric surveys. The sites were selected to accommodate the geometry needed for the exterior orientation (linking world and photograph coordinate systems) of blocks of overlapping photographs (multiple stereopairs along and between adjacent flight lines); each site was also accessible by helicopter. Most of the sites are part of a geodetic network established in 2000 (Dzurisin, 2003). Many are located near 3-m-high steel towers constructed after the 1980 eruption and used for electronic distance meter (EDM) surveys (Swanson and others, 1981). These towers or their shadows are relatively easy to find in the diapositive (film positives) rendering of aerial photographs used to help locate ground-control sites in the digital images. Using a helicopter and two crews, we were able to measure and place photo-targets at all of the stations in 1–2 days.

Measuring GPS locations in the field for ground control at Mount St. Helens is a straightforward task. We deploy a GPS receiver at each site, centering the antenna over a specific tower leg, piece of rebar, or benchmark. GPS receivers collect data at each site for about 1 hour. Before moving to the next site, three or four large plastic rectangular panels are placed radially about each GPS point to facilitate locating the control point in aerial photographs. The receiver data are downloaded and processed using Ashtech Office Suite for Survey ® (AOSS) software. The reference station for differential GPS processing is JRO1 (fig. 2*A*), which at the start of the eruption was the nearest continuous GPS station (approximately 9 km north of the crater). Altitudes from AOSS are converted to orthometric heights using the National Geodetic Survey (NGS) program GEOID03. The U.S. Army Corps of Engineer program CORPSCON is used to calculate X, Y, and Z coordinates using a horizontal datum of NAD83 and a vertical datum of NAVD88. The GPS data yield position accuracies of 2 to 3 cm in X and Y (horizontal) coordinates and 6 to 7 cm in the Z (vertical) coordinate.

Control points were remeasured annually from 2000 to 2004 before taking aerial photographs of the entire volcano. Repeated measurement improved and validated the positional accuracy of most sites. However, the landscape evolves quickly at Mount St. Helens, and site positions change, at times dramatically. For example, in 2002 the photo panels and rebar of the Brutus site on the east crater rim (fig. 2, station Br) were buried beneath about 20 cm of wind-blown pumice. The following year, the site toppled into the crater and had to be replaced.

New Ground Control Based on GPS Data and Photo-Identified Points

When the 2004–5 eruption began, four established flight lines used in previous studies to capture aerial photography of most of the volcano were abandoned in favor of a single, south-to-north flight line centered over the crater. A single flight line offered advantages of safety, simplicity, speed, and economy. However, it eliminated use of ground control points on the east and west outer flanks of the volcano and

forced reliance on control points on the crater rim, floor, outer south flank, and 1980s lava dome. Unfortunately, explosions early in the eruption eliminated three critical ground control sites on the 1980s lava dome (fig. 2*B*). Several of the remaining control points were outside the stereo coverage of the single flight line.

Rather than increase the number of flight lines and incorporate the ground control on the volcano flanks in an aerotriangulated block or replace the ground control in the crater's potentially dangerous environment, we transferred control points from the stored orientation solution (aerotriangulation) of the 2000 block of aerial photographs. Photoidentifiable, measured points (fig. 2*B*), such as distinct boulders or topographic prominences, were carefully selected and passed from the aerotriangulated solution of 2000 models to the 2004 aerial photographs as ground control. These points or a subset of them provided control for successive sets of photographs obtained throughout the winter of 2004–5. The resulting ground-control accuracy was reduced from a few centimeters, based solely on GPS data, to a few decimeters using photogrammetrically transferred control points.

In July 2005 we remeasured and repaneled the network of existing ground-control points on the crater rim and flanks. In addition, we reestablished one of the points on the west side of the 1980s lava dome and added points on the crater floor north of the 1980s lava dome and a site on the south crater rim (fig. 2*B*).

Aerotriangulation

Aerotriangulation provided a means of transferring accurate control from earlier photogrammetric work at Mount St. Helens, rather than establishing new control in hazardous areas as the eruption progressed. Aerotriangulation refers to solving relative orientation equations for overlapping aerial photographs (stereo model), identifying common points (pass points) between adjacent models to form continuous strips or blocks of stereomodels, and solving simultaneous equations to adjust mathematically the strips or block of photographs to ground control. A series of nonlinear expressions with many unknowns are truncated by Taylor's theorem into a series of linear equations that are solved simultaneously by the method of least squares (Wolf and Dewitt, 2000). Our 2000 benchmark DEM was created from an aerotriangulation solution for a block of aerial photographs. The block comprised four adjacent, overlapping strips of photos; each strip was formed from seven or eight overlapping photographs. Point coordinates extracted from the 2000 stereomodels and aerotriangulation were used as control points for successive stereomodels and for aerotriangulation solutions during the early part of the 2004–5 eruption. The resulting root-mean-squared (RMS) residual error for the early aerotriangulation solutions was a few decimeters. New and remeasured GPS ground-control points in the aerial photographs taken in the summer and fall of 2005 resulted in an aerotriangulation RMS residual error of several millimeters to several centimeters. The average RMS error from all aerotriangulation solutions was 0.17 m in the X, Y, and Z coordinates. Extending that error over the area that has been affected by the eruption (about 1 km^2) gives rise to a volume of uncertainty of 1.7×10^5 m^3. This error is about 4 percent of the typical monthly extruded volume (4×10^6 m^3) estimated from comparison of the series of DEMs (Iverson and others, 2006, Supplementary Notes).

Digital Elevation Model (DEM) Construction

We used spatial resection calculations to derive an aerotriangulation solution and then used spatial triangulation algorithms to extract three-dimensional coordinates and construct a DEM that defines the crater surface. Two techniques were used for obtaining X, Y, and Z coordinates from the stereomodels.

The first method was a manual technique that relies on the skill of the operator. The operator examined one or more stereomodels and identified the area being deformed and the features to be measured. For each feature, the operator carefully placed a floating mark on the feature, stored the Z (elevation) coordinate, and triangulated and stored the X and Y (planimetric) coordinates. Points were collected individually or as a stream as the operator moved the floating mark along the terrain.

The second method was an automated technique in which Socet Set software used coplanarity equations to derive a plane intersecting three points: (1) an object in one image; (2) the same object in the overlapping area of a second, adjacent image; and (3) the triangulated position of the object on the ground. The software used the line formed where the plane intersected the two adjacent photographs to guide its search for matching cell patterns. When the X and Y coordinates of matching cell patterns were identified, the software calculated the corresponding Z coordinate. The operator defined an area and density of points for the automated calculations. The automated method did not work well in steep terrain but did work in the relatively flat-lying, glacier-covered parts of the crater, provided there was enough contrast (such as a dusting of ash) in the photographs to provide unique cell patterns. The automated technique identified, calculated, and stored X, Y, and Z coordinates for many locations relatively quickly. This technique was used sparingly, however, because it can be labor intensive. Automatically generated points must be checked by the operator, either individually or by generating contours of groups of collected points, to correct any errors.

Using these two techniques, individual points or streams of points marking breaks in slope (breaklines) were collected to better define topographic inflections, enabling intervening surfaces on the growing dome and deforming glacier to be represented by significantly fewer data points. The resulting three-dimensional surface is an array of triangular

facets referred to as a triangulated irregular network (TIN), in which interpolated surfaces are triangles having measured points at each vertex. A TIN surface was checked for systematic errors or random operator error in a few seconds by generating digital contours for the surface. The operator easily located and repaired errors, such as points that caused contours to cross, and recalculated the TIN surface.

After error checking and visually determining that the TIN was an accurate representation of the three-dimensional surface depicted in the aerial photographs, the TIN data structure was stored and converted to a DEM. The DEM differs from the TIN in that the former is a regular array of square cells (or rasters), where each cell represents an area of the Earth's surface (X, Y) with a specific altitude value (Z). During this conversion process, the cell size or resolution did not dictate the accuracy of an altitude value. Rather, the resolution dictated how closely the DEM represents the TIN model. The accuracy of altitudes and horizontal positions was determined by the combined photogrammetric orientations, operator's skill, and in particular by the accuracy of the ground control.

Sources of error in the DEM construction included aerial camera calibration, film processing, flight parameters, ground control points, conversion of photos to digital form, stereomodel orientation (interior, relative, absolute), aerotriangulation, image-matching algorithms, operator bias, and random factors (Daniel and Tennant, 2001, p. 402–403). We estimated the uncertainty of any volume measurement to be a function of the area of the growing dome multiplied by the average RMS residual error (0.17 m). Thus, as the volume continued to increase, so did the estimated uncertainty of the volume calculation. However, the resulting uncertainty in volume-change calculations was about 4 percent—small compared to the ambiguity introduced by the unknown subsurface configuration of the lava dome (the lower part of the new dome masked by Crater Glacier).

Surface Depiction Using DEMs

The DEMs were imported into an ArcInfo Geographic Information System (GIS) for viewing and analysis after conversion to an ASCII text file in the softcopy system. This file, which was formatted for import to ArcInfo software, included a header containing the number of columns, number of rows, cell size, and X and Y coordinates of the lower left corner of the DEM, followed by a sequence in row-major order (top row first, bottom row last) of all the Z (elevation) values. The file was imported into the ArcInfo grid module as a high-resolution (2 m) grid (raster data structure).

Perhaps the most significant and primary use of any photogrammetrically constructed DEM is to examine the surface, either singly or in sequence with previous DEMs. Such a succession of DEMs for Mount St. Helens shows, qualitatively, the changing position, dimensions, and size of the growing dome and deforming glacier over time. The DEMs are difficult to examine or interpret directly. A hillshade algorithm was used to position an artificial "sun" at an arbitrary azimuth and altitude to render a gray-scale shaded-relief view of the changing dome and glacier. This rendition of the topography is free of potentially distracting details seen in the aerial photographs, such as steam, snow, or ash, and allows consistent and simplified viewing to study geomorphic change and compare cell alignment among DEMs.

The areal extent of the dome complex and deformed glacier increased throughout the 2004–5 eruption, forcing a corresponding increase in the extent of DEMs to document the change. To ensure proper alignment (registration) of the DEMs, they are cast within the same projection, same horizontal datum, and same vertical datum. We selected the Universal Transverse Mercator (UTM) projection's zone 10, which extends from 120° to 126° west longitude, the 1988 North American Vertical Datum (NAVD 88), and the 1983 North American horizontal datum (NAD 83). Previous DEMs derived from contours having a 1927 horizontal datum (NAD 27) were converted to NAD 83. In addition, a regional vertical correction of 1.25 m (Zilkoski and others, 1992) was applied to convert the 1929 vertical datum (NAGD 29) to NAVD 88. We confirmed this regional correction by calculating the difference between GPS control points stored in NAGD 29 and NAVD 88.

The extent of each DEM was varied in order to capture dome growth. Dome growth and the DEMs depicting the growth were bounded on the north by the relatively fixed 1980s lava dome and eventually bounded on the south by the south crater wall. The DEM edges on the east and west (as well as the south early in the eruption) were delineated visually to capture observed deformation, using the softcopy system. These results were confirmed by using GIS software to compare any current DEM to earlier DEMs. If we found that any of the DEMs had inadequate extent to represent the entire deformation field, the boundary could be extended using the scanned aerial photographs and aerotriangulation stored within the softcopy system.

Initially, the 2000 DEM was used as the baseline data set for all comparisons in order to keep the construction method consistent. However, the craterwide 2000 DEM had a cell size of 10 m, whereas DEMs constructed for the 2004–5 eruption had cell sizes of 2 m. The difference in cell size meant that each of the newer DEMs would have to be resampled to give a 10-m cell size. The error introduced by resampling outweighed the benefit of using consistent production methods; therefore, we later selected the craterwide 2003 DEM derived from lidar, and a 1986 DEM derived from contours, each having a 2-m cell size, for comparison with all subsequent DEMs.

Volume Calculation Methods

Although a single DEM surface offers a quick, synoptic portrayal of ongoing surface deformation, the comparison of successive DEM surfaces can yield estimates of erupted vol-

ume and average extrusion rate. We wrote software that uses GIS functions to subtract one DEM surface from another and generates a third, isoline surface showing net elevation change. The isoline surface stores the calculated difference between its two parent surfaces, retaining their 2-m cell size. In this manner, each cell of the isoline grid stores a positive, zero, or negative value resulting from the subtraction of the two corresponding parent cells. After the subtraction, the software sums values of all cells having a negative value (melting, erosion, or subsidence) and of all cells having a positive value (extrusion, deposition, or uplift) separately, and it also multiplies each total positive or total negative value by the area of a single cell (4 m^2). The software writes the resulting volumes to a text file and generates two additional grids, one showing the location of the positive and another showing the location of the negative results.

The potentially straightforward task of determining extruded volume from total-volume changes was complicated by the presence of Crater Glacier, in some places more than 150 m thick (greater than 200 m thick when including subglacial 1980–86 crater-floor deposits), which was displaced and severely disrupted as the eruption progressed. Two questions arose: (1) Does extrusion begin at the preexisting crater floor or at the glacier surface; and (2) how best to calculate erupted volume as a function of time? One approach (fig. 3*A*) is to difference each new DEM with the 2003 preeruption DEM and to use the total surface-volume change as a proxy for erupted volume. For example, 1 m^2 of glacier ice rising 2 m represents 2 m^3 of lava extruded beneath it or laterally displacing it. This approach has the advantage of accounting for all material that rose above the crater floor, some of which remains obscured by ice, and the method is simple and straightforward. Three disadvantages of this total volume-change technique are the unknown total amount of dilatation caused by ice deformation (though the largest crevasses are captured during DEM construction), volume gain by winter snow accumulation, and volume loss by melting.

Another approach (fig. 3*B*) is to assume that lava extends from the lava-ice contact at the surface vertically downward to the 1986 crater floor. This is a reasonable approach for three reasons: (1) field examples of ice-contact lava flows have steep sides that formed as they flowed against steep ice walls (Lescinsky and Fink, 2000); (2) where observed around the Mount St. Helens dome, ice-lava contacts are nearly vertical; and (3) this method is also simple and straightforward. One disadvantage is that this method ignores observed rising crater-floor material or glacier, especially early in the eruption, which probably deform in response to endogenous or subglacial lava emplacement.

Our solution was to use both approaches to track volume estimates. The first approach provided measurements of extruded rock independent of whether rock broke through the glacier surface. As the eruption proceeded, the dome grew larger and the impact of the glacier became proportionally smaller. The discrepancy between the two approaches therefore decreased over time.

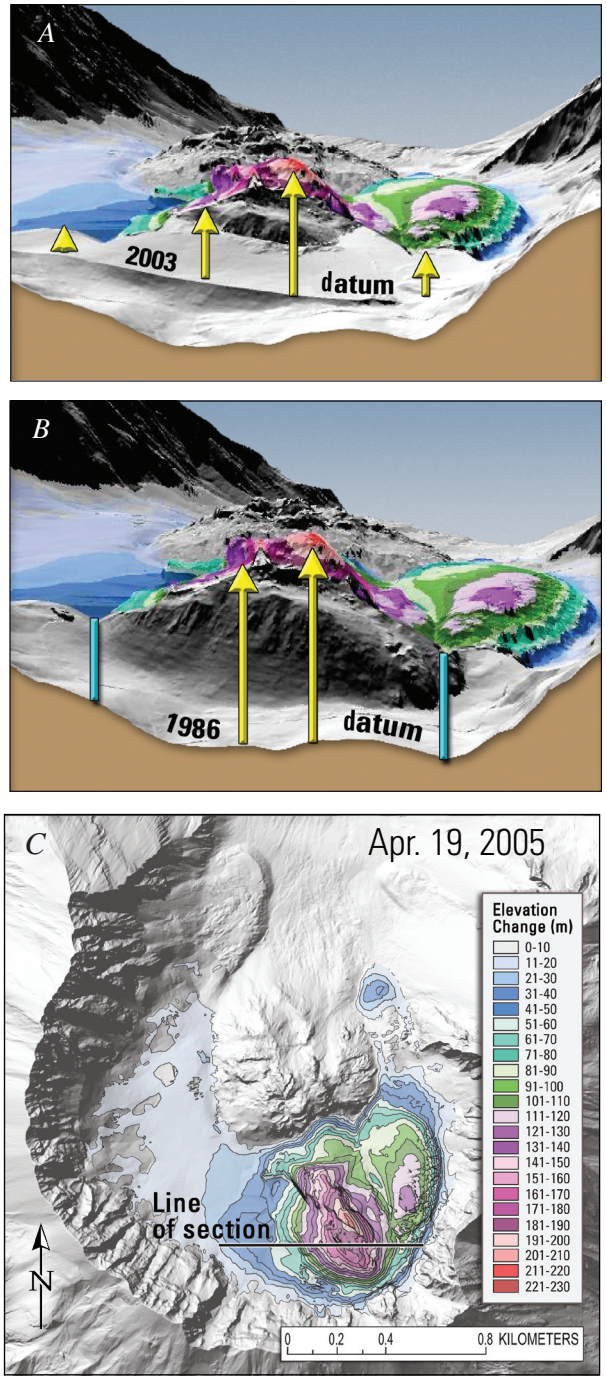

Figure 3. Diagrams (*A, B*) illustrating DEM differencing for volume-change calculations. Semitransparent oblique cutaway of surface defined by April 19, 2005, isolines (colored bands) draped on DEM showing 1986 ground topography and 2003 glacier surface. Yellow arrows, examples of local elevation changes. View to north-northwest. *A*, Total volume change. Note that differencing includes marginal areas, unlikely to be underlain by lava, that are composed of deformed glacier. *B*, Extruded-lava volume. Blue bars define inferred steep margins of extrusion. *C*, DEM and differencing surface of April 19, 2005. The DEM and differencing surface south of the line of section were removed to produce oblique views *A* and *B*.

Results

A sequence of 17 pairs of images derived from DEMs of October 4, 2004, through December 15, 2005, document lava dome growth and glacier deformation during the 2004–5 eruption (figs. 4, 6–8). For each pair, the left image is a shaded-relief map. Beginning with the October 13, 2004, map, a red line marks the approximate boundary of extruded lava on the surface that was extended vertically to the 1986 crater floor to calculate the extruded-lava volume. The right image is an isoline map draped over the shaded-relief image. Each 10-m interval of the isoline map is assigned a unique color to illustrate better the magnitude and location of elevation change relative to the 2003 crater surface. All isoline cells having an elevation difference equal to or greater than 10 m were summed to calculate total volume change. Some of the shaded-relief images, such as that for October 11, 2004 (fig. 4*E*), have triangular facets that portray areas where a

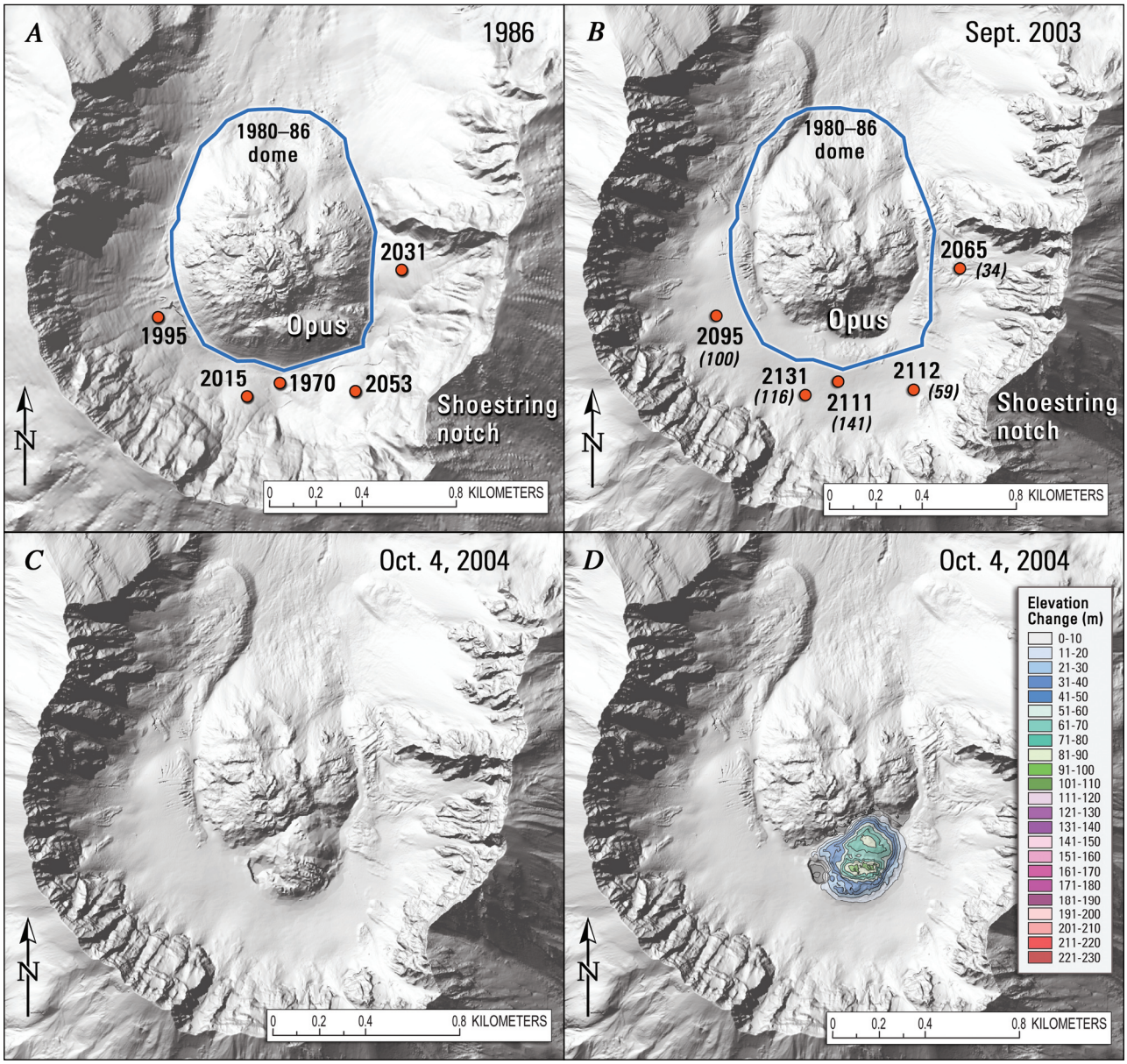

Figure 4. Shaded-relief images showing preeruption crater surface and growth of welt and initial lava extrusion (red outline in *G*). *A*, 1986 and *B*, 2003. Blue line, approximate boundary of 1980s lava dome. Red dots show altitude, in meters, of points on crater floor. Increases (in parentheses) caused by growth of Crater Glacier and deposits eroded from crater walls. Area labeled Opus is part of the 1980s lava dome involved in uplift in late September and early October 2004. *C–H*, sequence of three pairs of images from October 2004. Left image is shaded relief map; right image has 10-m isolines showing topographic changes relative to September 2003 (shown in *B*).

condensed steam plume in the aerial photographs prevented detailed coordinate collection.

Also shown for reference in figure 4 are shaded-relief images of the craterwide datum surfaces from 1986 (fig. 4*A*) and 2003 (fig. 4*B*). The shaded-relief map of the 1986 crater shows the configuration of crater walls, talus fans and other deposits on the crater floor, and the 1980s lava dome. The 2003 shaded-relief map also shows the newly formed glacier, which buries some margins of the 1980s lava dome. Spot altitudes show the magnitude of surface-elevation change from 1986 to 2003.

As the new lava dome grew, questions about the volume of the 1980s lava dome arose. We differenced DEMs to estimate a volume of 92×10^6 m^3 for the 1980s lava dome (Thompson and Schilling, 2007), which is larger than the 74×10^6 m^3 estimate of Swanson and Holcomb (1990) but is in agreement with volume calculations of Mills (1992). The difference in volume estimates may result from (1) differences in measurement methods, (2) exclusion by Swanson and Holcomb (1990) of crater-wall debris that was incorporated into the dome as it grew (Mills, 1992), and (3) different configurations for the base of the lava dome as a horizontal versus sloping surface.

The following discussion of the DEMs focuses on four time intervals and highlights key events related to dome building and deformation of Crater Glacier: (1) Growth of the so-called welt (Dzurisin and others, 2005), south of the 1980s lava dome, and its migration southward in late September and early October 2004 involved uplift of a part of the 1980s lava dome (area labeled Opus on figs. 4*A*, 4*B*),

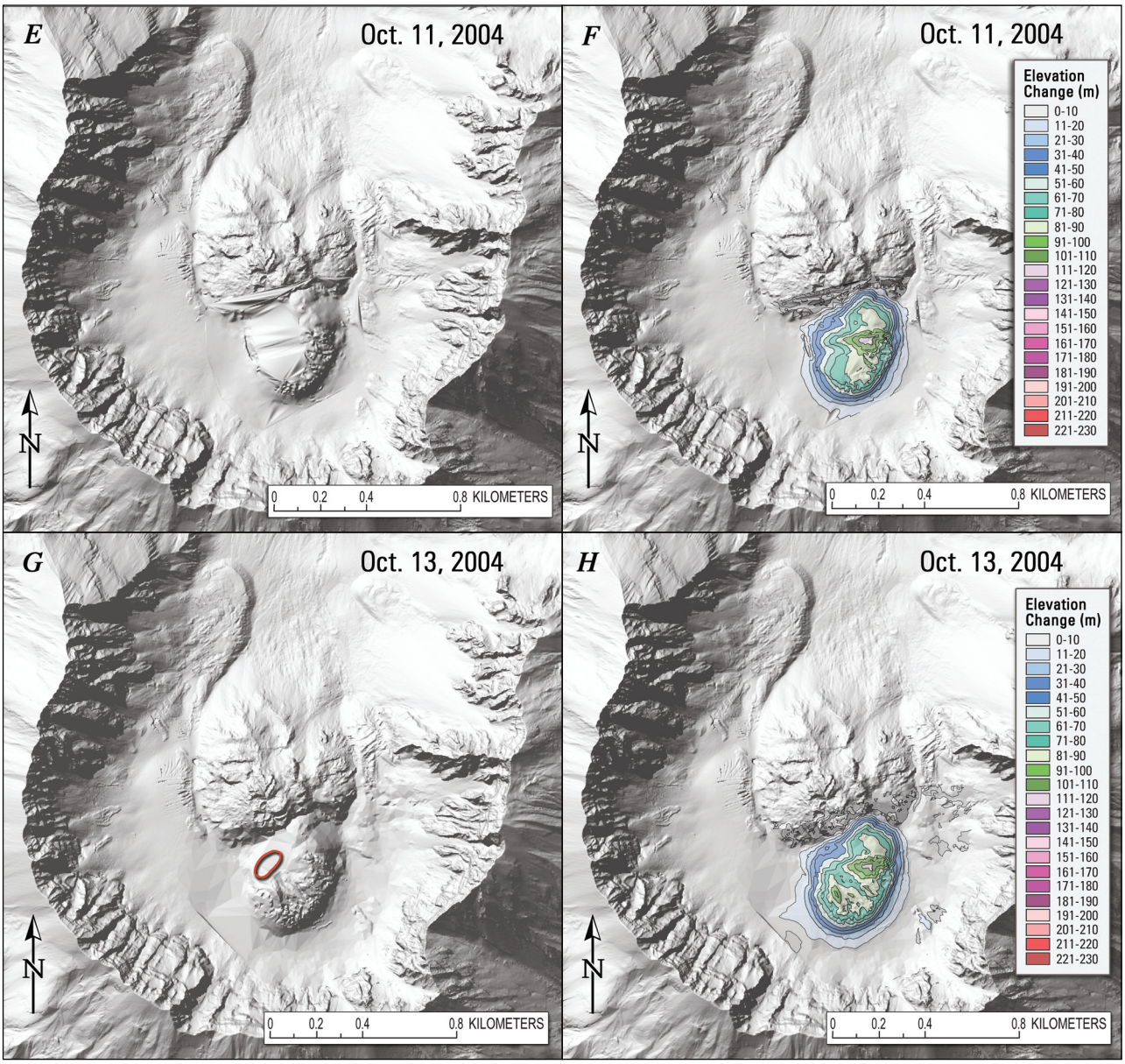

Figure 4—Continued.

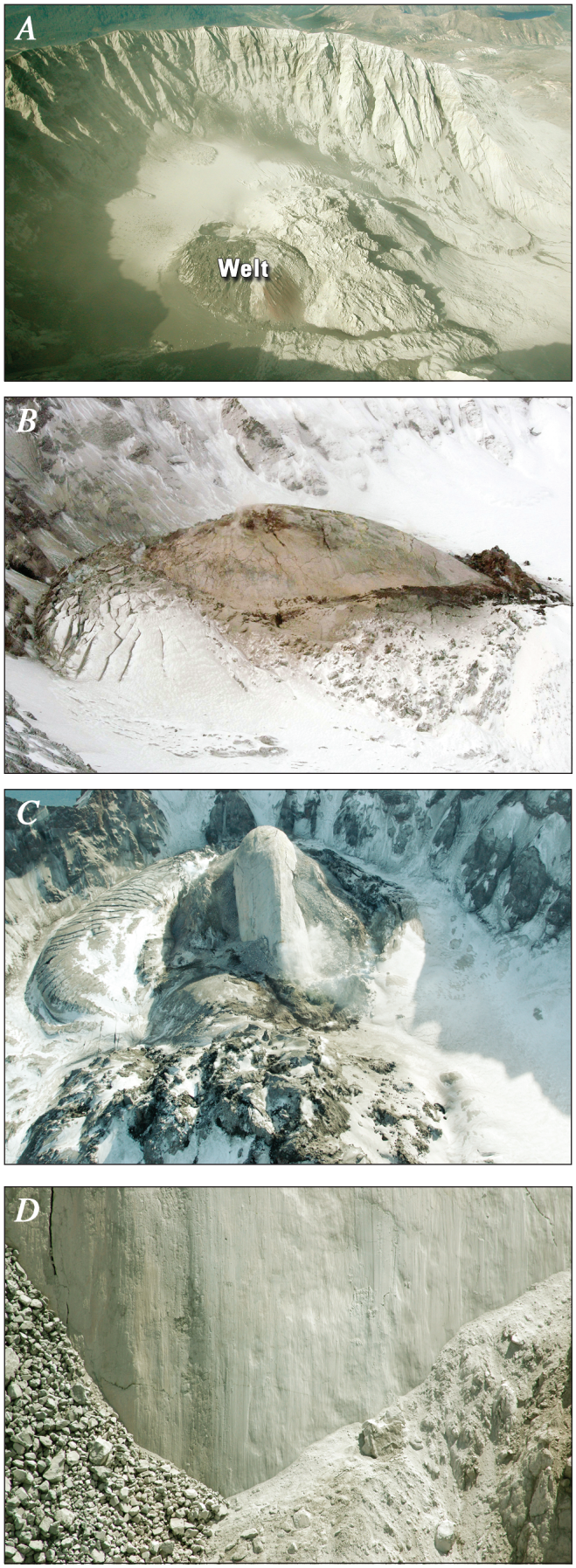

crater-floor debris, and glacier ice. Initial lava spines 1 and 2 (see Vallance and others, this volume, chap. 9, for description of the lava-spine numbering scheme) rose through the northern part of the welt near the end of this interval. (2) From late October 2004 through mid-April 2005, extrusion, growth to the south and migration east, and breakup of curvilinear, smooth-surfaced spines 3 and 4, known as whalebacks, drove extraordinary deformation of the east Crater Glacier. The first evidence of lateral movement of the spines came from the DEMs. For example, the extrusion axis, a horizontal line oriented parallel to the direction of extrusion along the approximate center of a whaleback, initially moved southward, then shifted eastward from October 2004 through April 2005 (approximately 4° horizontal rotation of the whaleback axis towards the east occurred between November and December 2004 and about 6° between February and March 2005), as successive whalebacks emerged from the vent area, displacing older parts of the growing dome. (3) Between mid-April and late July 2005, smooth-surfaced spine 5 grew at a much steeper angle than had the previous whalebacks and began a trend toward west-directed movement. (4) In August 2005 spine 6 began to grow and migrate westward, followed by penetration of its eastern part by spine 7 in early October. Both spines moved west, which compressed and thickened west Crater Glacier. For a complete description of the geologic interpretation of dome growth, see Vallance and others (this volume, chap. 9). For a complete description of glacier deformation, refer to Walder and others (this volume, chap. 13).

October 4 Through October 13, 2004

Recognition of the welt (Dzurisin and others, this volume, chap. 14) a few days after seismic unrest began on September 23, 2004 (Moran and others, this volume, chap. 2), prompted efforts to obtain DEMs of the crater. The first group of images (figs. 4*C–H*) shows the remarkably rapid

Figure 5. Photographs of 2004–5 dome. *A*, View of crater after explosion of October 5, 2004. Welt formed of uplifted glacier, crater-floor debris, and southeast part of 1980s lava dome. Light-gray ash covers most of crater. View to west. *B*, Recumbent spine 3 on November 29, 2004, after impinging upon southeast crater wall. Its smooth carapace and leading wave of deformed glacier ice inspired the descriptive term, whaleback. View to southwest. *C*, Crater on February 22, 2005, showing spine 4 flanked by talus and, to left, remains of spine 3. Highly deformed east Crater Glacier prominent in left part of photograph. View to south. *D*, Close-up view about 5 m across of gouge-covered spine 4 extruding from vent, May 12, 2005. Striations parallel the direction of motion. Talus flanking spine is covered by dust from rockfalls and sloughing of gouge on right. View to south. USGS photographs by S.P. Schilling (*A, C, D*) and S. Konfal (*B*).

Table 1. Total volume change, extruded lava volume, and rates of change during 2004–2005 eruption of Mount St. Helens.

[Extruded lava did not appear at the surface until October 11, 2004. Rates are calculated from the volume changes since the previous measurement.]

Date of photography	Total volume change (x 10^6 m^3)	Total volume change rate (m^3/s)	Extruded lava volume (x 10^6 m^3)	Lava extrusion rate (m^3/s)
10/4/2004	5 [1]	-- [1]	-- [2]	-- [2]
10/11/2004	10	8.9	-- [3]	-- [3]
10/13/2004	11	6.4	0.54 [4]	-- [4]
11/4/2004	20	4.6	12	5.9
11/29/2004	27	3.0	21	4.4
12/11/2004	30	3.4	26	4.1
1/3/2005	35	2.4	31	2.5
2/1/2005	40	1.9	35	1.8
2/21/2005	43	1.8	39	2.4
3/10/2005	45	1.5	42	1.8
4/19/2005	55	3.0	47	1.5
6/15/2005	59	0.8	54	1.4
7/14/2005	59	-0.2	57	1.3
8/10/2005	60	0.4	62	2.0
9/20/2005	62	0.7	67	1.6
10/24/2005	66	1.3	70	0.9
12/15/2005	75	1.9	73	0.7

[1] Volume is the welt, obtained by method of differencing from topographic surface of September 2003. Start date for growth of welt is imprecisely known, so no rate offered.

[2] Eruption has not begun; no extruded lava.

[3] Too steamy to confidently discern limits of new extrusion.

[4] Steamy; extruded lava volume is crude estimate, and no rate is offered.

changes that occurred in 10 days as the welt grew rapidly upward and southward, deforming parts of the 1980s lava dome, crater-floor material, and Crater Glacier (fig. 5*A*). By October 11 the welt had grown to about 425 m in width, 475 m in length, and 105 m in height (2,209 m altitude) above the 2003 glacier surface. (Length of welt and dome is measured along the approximate longest dimension of each shape, and width is measured along a line roughly perpendicular to the length.) The welt attained a volume of 10×10^6 m^3 (table 1) as lava spine 1 emerged on October 11 (Vallance and others, this volume, chap. 9; Pallister and others, this volume, chap. 30). Presumably the volume of the welt approximated the volume of lava emplaced onto the subglacial crater floor.

November 4, 2004, Through April 19, 2005

Nine image pairs (fig. 6*A*–*P*) show the sequential growth of lava spines 3 and 4, which shared a similar history in terms of form, growth, and demise. These two striated, gouge-covered, curvilinear, whaleback-shaped spines (figs. 5*B*, 5*C*, 5*D*) grew south-southeast from the vent. The southern ends were pushed eastward over time and broke apart after impinging upon the south crater wall. Both whalebacks were surrounded by talus aprons on the west, south, and east. Initially the disrupted glacier adjacent to the talus aprons formed a crevassed ridge that, in map view, looked like the bow wave of a ship (figs. 6*A*, 6*C*). West of the growing dome, the talus apron, gently flexed ice, and intervening depression formed a relatively stable configuration throughout this period.

The November 29, 2004, image (fig. 6*C*) shows that lava spine 3 had a wide center with tapering ends. It was about 145 m wide, 350 m long, and at its highest point 150 m above the 2003 surface (altitude 2,282 m). The December 11, 2004, image (fig. 6*E*) shows that a longitudinal fracture had formed and broken the whaleback into two parts. By January 3, 2005, prominent longitudinal and oblique transverse, northwest and north-northeast-striking fractures had broken spine 3 into many blocks, presumably as a result of the spine impinging on the south crater wall (Vallance and others, this volume, chap. 9). The resulting 31×10^6 m^3 dome was about 500 m long by 200 m wide and reached 184 m above the 2003 crater surface (altitude 2,293 m). East Crater Glacier was squeezed between the grow-

ing dome and the southeast crater wall (figs. 6*C*–*H*), becoming severely disrupted as it thickened more than 120 m into a conical form by December 11, 2004 (figs. 6*E*, 6*F*). The highest area of disrupted ice shifted about 100 m to the northeast by January 3, 2005 (figs. 6*G*, 6*H*). The west Crater Glacier experienced broad uplift of about 10 m near the 1980s lava dome and near the south crater wall (figs. 6*D*, 6*F*, 6*H*).

A second whaleback (spine 4) began forming in early January 2005 from the severed stump of spine 3. By February 1 it was 145 m wide, 320 m long, and 210 m above the 2003 surface (altitude 2,331 m) (elevation of corresponding point on 2003 surface varies slightly as location of high point of whalebacks changes) (figs. 6*I*, 6*J*). These dimensions are similar to those of spine 3 on November 29, 2004. Spine 4 grew south-southeastward to about 450 m in length, 150 m in width, and 210 m (altitude 2,343 m) above the 2003 surface on March 10, 2005 (figs. 6*M*, 6*N*). As with spine 3, longitudinal fractures cut the southwest edge of spine 4 (fig. 6*M*). In April 2005, longitudinal, northwest-striking fractures and oblique transverse, northeast-striking fractures broke spine 4 as it impinged on the south crater wall, forming rubble and several megablocks (fig. 6*O*).

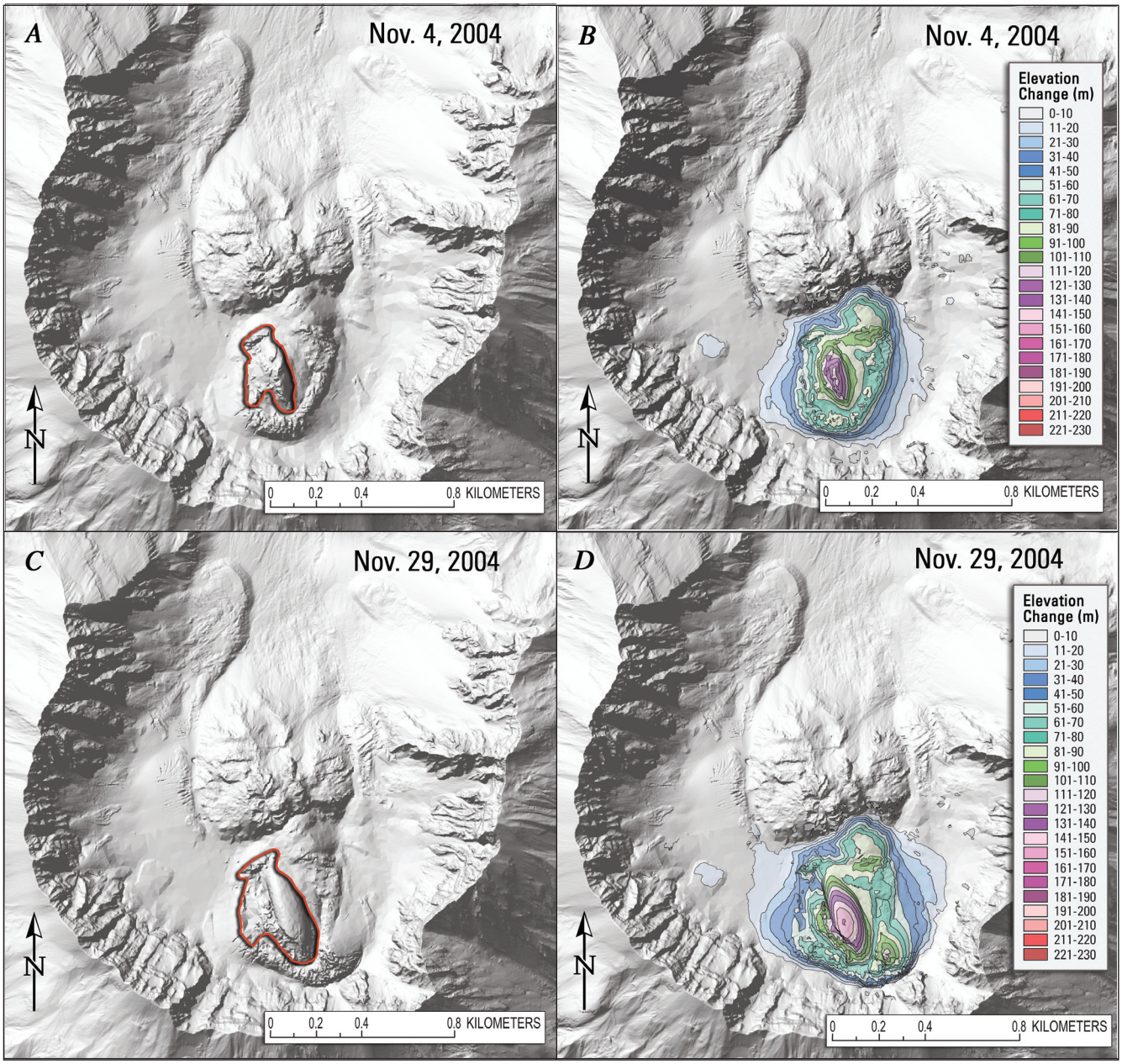

Figure 6. Sequence of eight pairs of shaded-relief images (*A*–*P*) showing growth of lava dome complex (red outline) and deformation of Crater Glacier from November 2004 to April 2005. Arrows (panel I) shows prominent, arcuate step on east Crater Glacier. For full explanation, see figure 3 and text.

The corresponding isoline maps for this time period show the response of the glacier to the growing dome (figs. 6*J*, 6*L*, 6*N*, 6*P*) as an increasing number of en echelon, east-trending, transverse crevasses cut east Crater Glacier. Apparent counterclockwise rotation and thickening of the glacier west of Shoestring notch to more than 110 m above its former surface in 2003 was in response to the dome-glacier margin moving eastward. In March 2005, a second small area of glacier ice had reached a similar height (fig. 6*N*) and, by April, an area about 100 by 50 m had attained a height of more than 120 m above the 2003 surface (fig. 6*P*).

Between late February and April, new crevasses oblique and perpendicular to the existing crevasses cut the southern part of the glacier into blocks (fig. 6*O*). A prominent east-west, arcuate, steplike feature (figs. 6*I–P*; highlighted by arrows on fig. 6*I*) about 30 m high formed at the glacier surface east of the 1980s lava dome (see discussion in Walder and others, this volume, chap. 13). This ice step was cut by short radial crevasses. The broad thickening of west Crater Glacier continued primarily along the southwest edge of the 1980s lava dome. For example, the 20-m isoline lay about 130 m farther northwest in April than in February (figs. 6*J*, 6*P*).

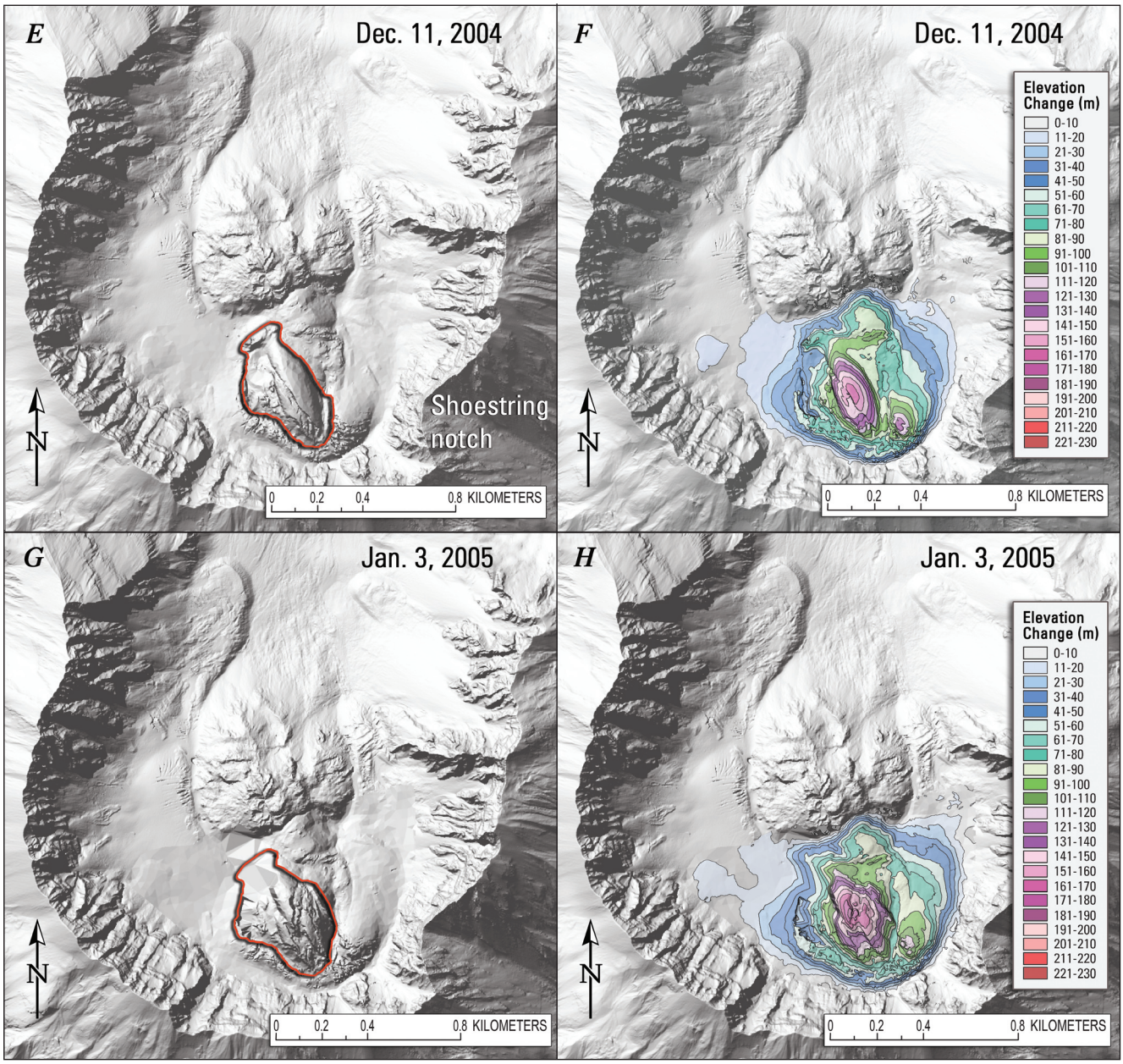

Figure 6—Continued.

June 15 Through August 10, 2005

The third group of image pairs (fig. 7*A*–*F*) shows that dome growth began to migrate west from its previous locus in the southeastern part of the crater. Though it is obscured in the June image (fig. 7*A*), the July image (fig. 7*C*) shows spine 5 was shorter (145 m in length), narrower (100 m across at the base), and higher (altitude 2,352 m, 250 m above the 2003 glacier surface) than the previous two spines, and it sloped steeply (about 60°) in all directions (see Vallance and others, this volume, chap. 9). Talus filled the substantial trough between west Crater Glacier and the dome that had existed for more than six months, eventually spilling onto the glacier surface. The slope angle of the talus on the northwest part of the new dome was about 32°. In July, spine 5 attained a height of 260 m (altitude 2,368 m) above the 2003 surface—the highest measured so far and within 2 m of the altitude of Shoestring notch, the lowest point on the crater rim. In August the dome was about 700 m in length and 600 m in width, with a volume of 62×10^6 m^3. Throughout the summer, crevasses continued to increase in number, disrupting the east Crater Glacier surface south of the prominent step, and they appeared in the elongate terminus of the glacier for the first time (fig.

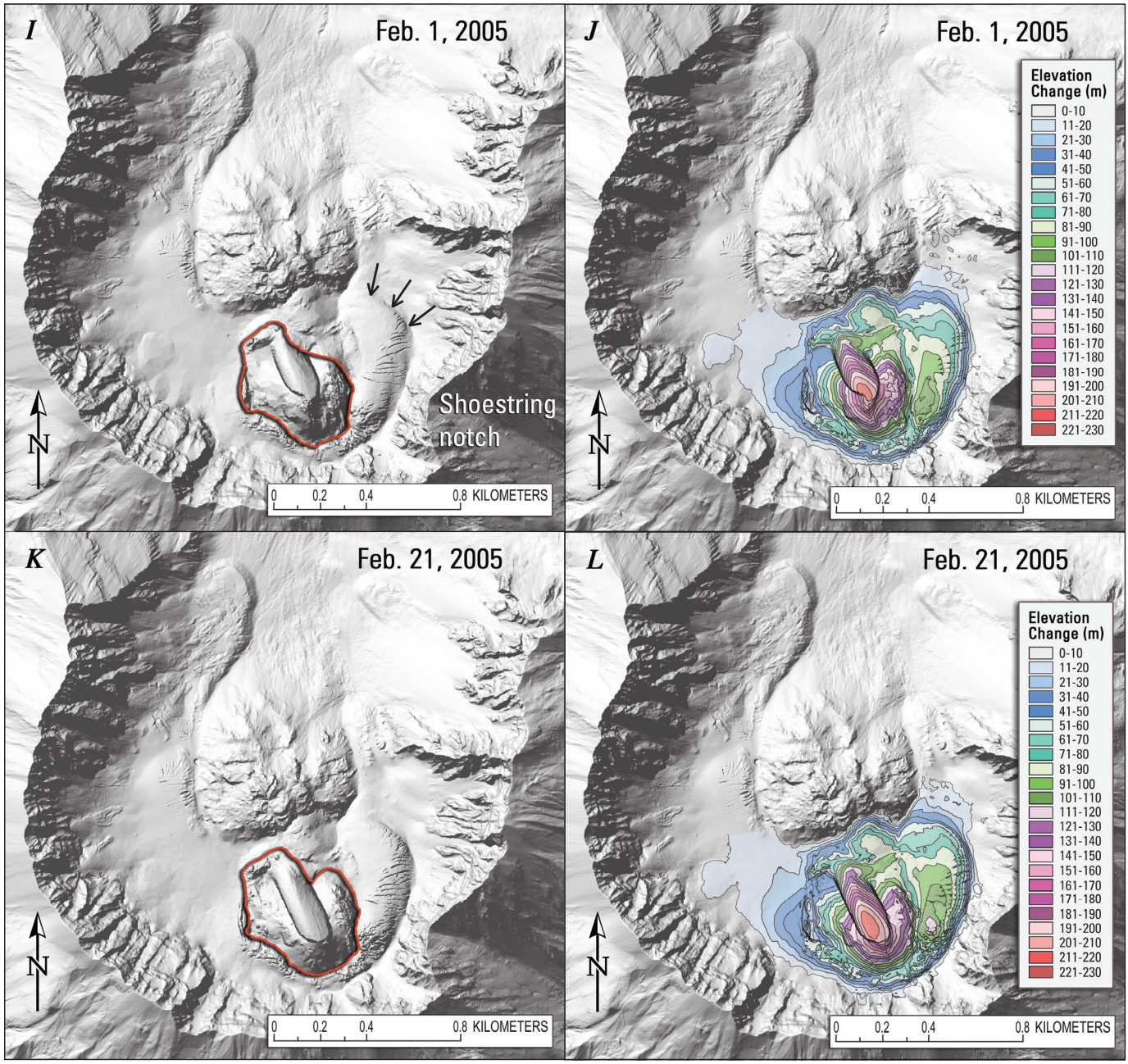

Figure 6—Continued.

7*A*–*F*). The effect of the northward advance of east Crater Glacier's terminus was to create an island of increased elevation shown by a series of closed isolines (for example, fig. 7*B*) (Walder and others, this volume, chap. 13). The isolines on west Crater Glacier indicate that thickening had slowed. However, subtracting the June 14 glacier surface from the July 15 glacier surface yields a negative change in volume (-1.5×10^6 m^3), likely a result of glacier melting. The west Crater Glacier-dome contact migrated about 60 m west between March and August, and radial and circumferential crevasses formed along the southeastern edge of the west glacier.

September 20 Through December 15, 2005

The fourth group of image pairs, (fig. 8*A*–*F*) shows that the locus of new dome growth migrated about 200 m west between August 10 and September 20, 2005. Part of spine 5 had decreased in elevation by about 75 m, forming a depression. Between September and December, spines 6 and 7 continued to grow westward, and the depression became a well-defined trough separating the newest growth from earlier spines. Spine 6 is difficult to distinguish within its flanking talus (fig. 8*A*), but it extruded on the northeast end of an elongate, arcuate ridge trending southwest along

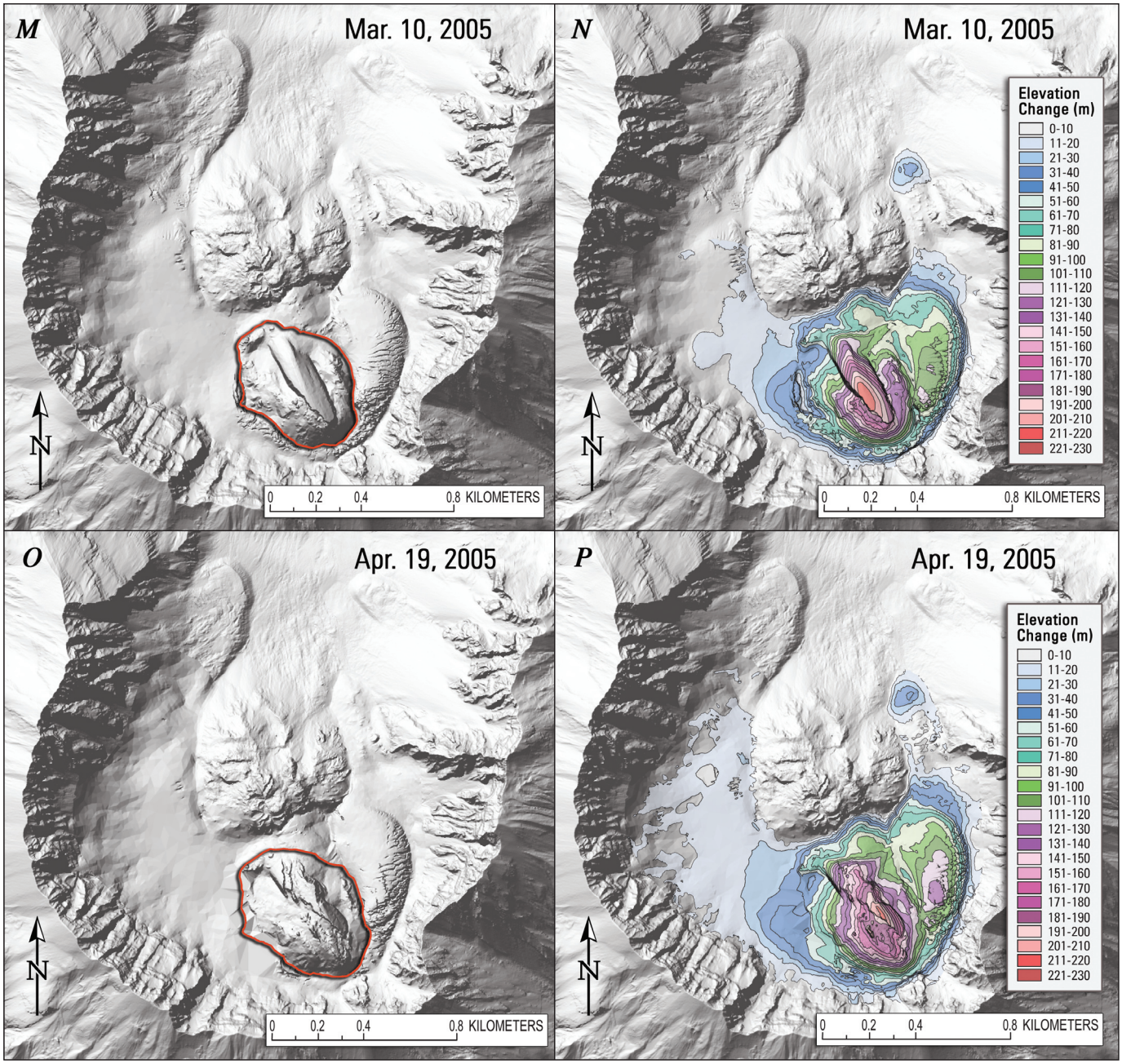

Figure 6—Continued.

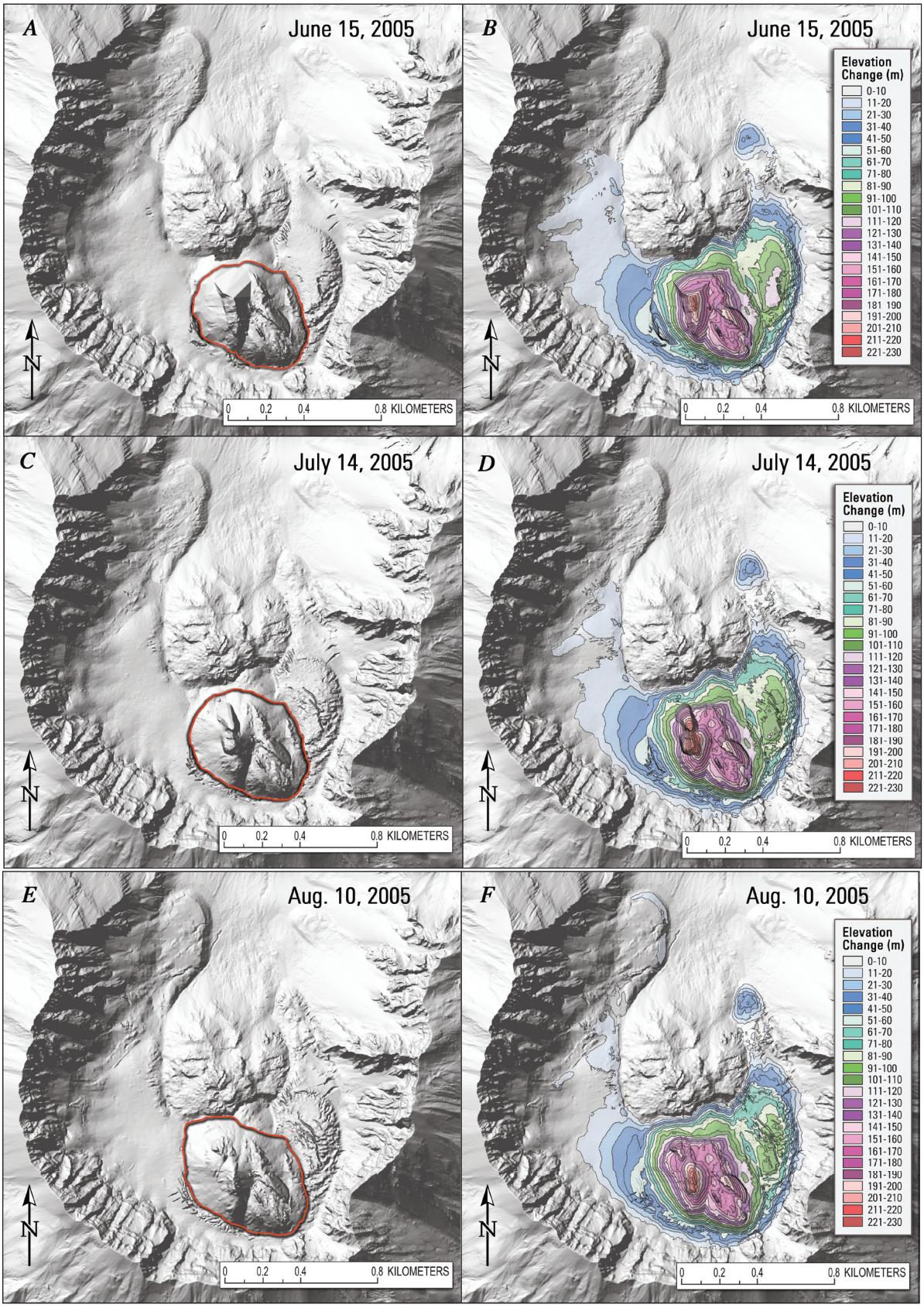

Figure 7. Sequence of three pairs of shaded-relief images (*A*–*F*) showing growth of lava dome complex (red outline) and deformation of Crater Glacier from June to August 2005. For full explanation, see figure 3 and text.

the top of the talus. In September, this newest part of the dome was about 420 m long, 285 m wide, and about 170 m (2,274 m altitude) above the 2003 glacier surface. By October, the highest point of spine 6 had migrated about 85 m west. Between October and December, spine 7 penetrated the eastern side of spine 6 and extruded upward and westward, bounded by a well-defined, nearly planar, gouge-covered surface striking approximately north-south. The nearly circular mass of talus and spines 6 and 7 was 430 m in length, 425 m in width, and about 180 m (altitude 2,280 m) above the 2003 surface. By December 2005, the entire dome complex was about 900 m long, 625 m wide, and 190 m (altitude 2,316 m) above the 2003 surface. Its volume, 73×10^6 m^3, was nearly equal to the 74×10^6 m^3 volume estimate of erupted lava for the 1980s lava dome (Swanson and Holcomb, 1990). East Crater Glacier was severely disrupted by both crevasses and summer ablation. The west glacier-dome contact migrated about 100 m west between September and December. Large crevasses formed on the west glacier, most likely in response to westward dome growth (Walder and others, this volume, chap. 13). Radial and circumferential crevasses increased in both size and number between September and December until the part of the glacier adjacent to the new dome took on the appearance of the disrupted east glacier. A prominent linear step, similar to the one on the east glacier, had migrated about 100 m north, and a broad area immediately south of the step had risen about 40 m.

Discussion

DEMs constructed from vertical aerial photographs provided an effective means to track and quantify dome growth and to calculate average magma-discharge rates of the 2004–5 lava dome at Mount St. Helens, as well as to gauge deformation of Crater Glacier. The DEMs met commonly identified needs in being (1) accurate—satisfying the appeal for precise, high-quality measurements at growing domes (Newhall and Melson, 1983); (2) safe—"acquired at low risk, and consequently * * * an important element in monitoring future activity of potentially explosive volcanoes" (Moore and Albee, 1981, p. 127); and (3) relatively inexpensive—acquisition costs of vertical aerial photographs and high-resolution scans are about 5 to 10 percent of those of other technologies such as lidar. Below we highlight suggestions for use of this technique at future eruptions, point out how DEMs and extruded-volume and extrusion-rate data were used in other studies, and draw a few brief comparisons between this and other dome-building eruptions.

Importance of Preparation and Suggestions for Improvements

Accurate measurements of the dome and glacier at Mount St. Helens were possible during even the critical earliest part of the 2004–5 eruption because we had baseline data and photogrammetric infrastructure in place before the eruption began. An earlier study of Crater Glacier (Schilling and others, 2004) had (1) identified an experienced photogrammetric contractor that ensured accuracy in camera calibration, film processing and scanning, and critical flight parameters such as altitude; (2) developed skills using aerotriangulation to orient blocks of photogrammetric stereomodels and to collect breaklines and points to create DEM surfaces with minimal operator bias and error; and (3) most importantly, established a network of ground control points on the flanks and crater floor of Mount St. Helens, validated by repeated measurements, with locational accuracy of a few centimeters. Hazards in the crater and uncertainty about the course of the eruption during late September and early October 2004 would have limited our ability to establish ground control. In retrospect, a greater number of control points in the crater area would have been useful, both to replace sites that were destroyed by explosions early in the eruption and to establish a set of points that could be remeasured to evaluate the accuracy of successive DEMs.

We spent days to weeks constructing each detailed DEM presented in this report, but, especially early in the eruption, a two-stage approach would have been advantageous to balance the need for rapid measurements for hazard-assessment purposes versus a greater level of detail for in-depth studies. Initial work would capture the minimal detail needed to obtain preliminary volume and extrusion-rate measurements. Later, as time allowed, we could add greater detail and improve accuracy.

Average Extrusion Rates

Plots of volume through time, whether comparing new crater-surface topography to the relatively uniform 2003 glacier surface (total volume change) or lava-dome volume as defined by the vertical projection of the dome outline to the 1986 crater floor (extruded volume), show that volume increased quickly early in the eruption and more slowly thereafter (fig. 9; table 1). Early in the eruption, measurements of total volume change document the deformation of glacier ice and existing crater floor to form a prominent welt (Dzurisin and others, 2005) having a volume of 10×10^6 m^3 and a growth rate of 8.9 m^3/s before lava first appeared at the surface on October 11, 2004. This volume estimate may be a minimum, because steam obscured some of the vent area. After the appearance of dacite lava at the surface, lava extrusion rates were initially 5.9 m^3/s, slowing to 2.5 m^3/s by the beginning of January 2005. After early 2005, the extrusion rate gradually declined to about 0.7 m^3/s, with a minor increase in rate during late summer 2005, and the total extruded volume gradually increased to 73×10^6 m^3 near the end of 2005.

For much of the eruption, the extruded-lava volume derived from the DEMs was the most appropriate measure of dome growth. However, especially early in the eruption, the unique situation of a lava dome erupting through a glacier required a second method, which included a measure of the total volume of surface deformation. This value was the sum of extruded volume and other surface volume change owing

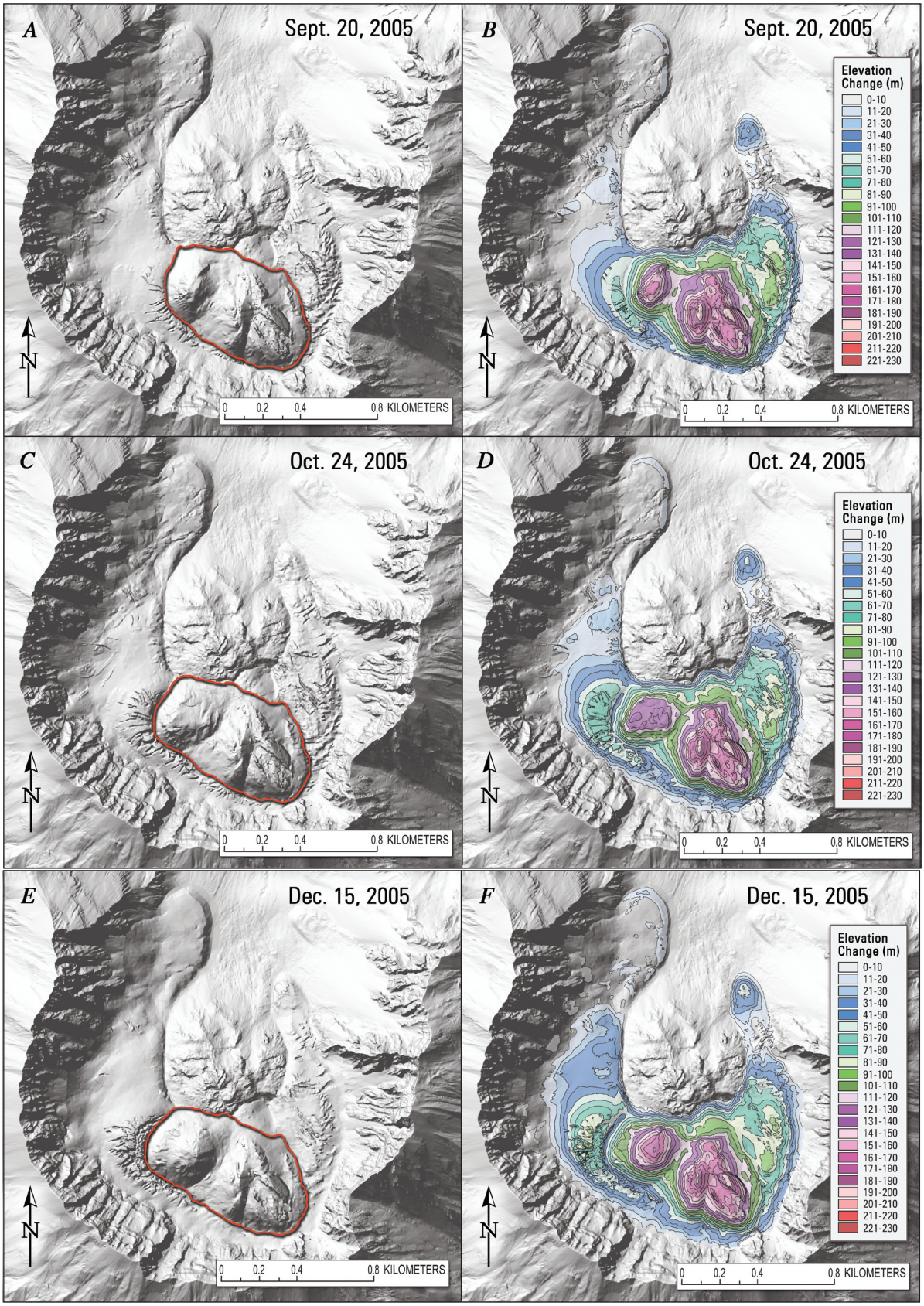

Figure 8. Sequence of three pairs of shaded-relief images (*A* –*F*) showing growth of lava dome complex (red outline) and deformation of Crater Glacier from September to December 2005. For full explanation, see figure 3 and text.

to deformation, snow and ice removal or accumulation, and addition of new talus from the crater walls. As the eruption continued, we used the extruded-lava volume to track dome growth and used the total volume change mainly to track changes in the glacier. Differences between the two rates resulted from factors unrelated to lava extrusion. For example, a prominent increase in the volume change rate in April 2005 (fig. 9*B*) coincided with including a larger part of west Crater Glacier in the April DEM, which resulted in adding more thickened glacier and seasonal snowfall to the total volume. A notable decrease of total volume change during a period of low extrusion rate during the summer of July 2005 likely reflects summer snowmelt and glacier ablation. The apparent slight increase in the extruded-lava rate in August 2005 is likely real.

Use of DEMs and Volume and Extrusion-Rate Data in Studies of the 2004–2005 Eruption

Vertical aerial photographs and the DEMs derived from them constitute one of the most widely used data sets collected during the 2004–5 eruption of Mount St. Helens. Scanned versions of the vertical aerial photographs provided a consistent base for interpretation and construction of photogeologic maps (Herriott and others, this volume, chap. 10). The DEMs provided numerical constraints to solve equations needed to estimate linear extrusion rates from a single remote camera (Major and others, this volume, chap. 12). Coupling the aerial photographic documentation with fields of deformation vectors and profiles of the dome derived from the DEMs yielded evidence to interpret the mechanics of dome growth (Vallance and others, this volume, chap. 9). Measurements and profiles from the DEMs helped to track the remarkable deformation of east and west Crater Glacier and showed that relatively little ice has been melted by dome growth (Walder and others, this volume, chap. 13).

Measurements of dome volume and extrusion rate were combined with other data sets such as seismology, gas geochemistry, and ground deformation to better understand eruptive processes. As the eruption continued, the extrusion rate remained relatively constant, even though the character of seismicity varied, suggesting that earthquakes were controlled more by changes in extrusion mechanics than by changes in extrusion rate (Moran and others, this volume, chap. 2). The

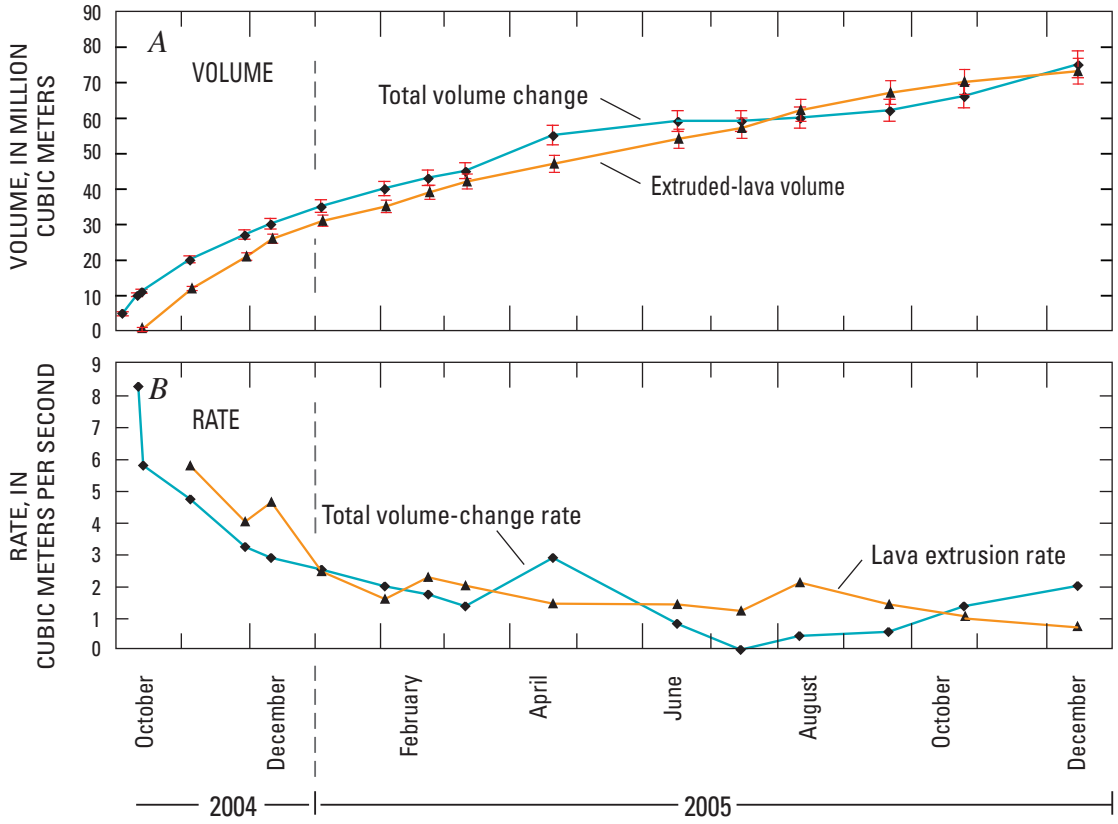

Figure 9. Time-series plots of dome growth at Mount St. Helens from start of eruption through December 2005. *A*, Total volume change (blue line) and extruded-lava volume (orange line) versus time. *B*, Total volume change rate (blue line) and volumetric extrusion rate (orange line) versus time. Early in eruption, all surface deformation likely resulted from extrusion or shallow intrusion of lava into glacier, and total volume change therefore would approximate lava extrusion rate.

nearly constant extrusion rate was also a key observation incorporated into a mechanistic model of extrusion driven by a nearly constant influx of magma from depth and resisted by a plug of solidified magma that slipped incrementally against the walls of the conduit (Iverson and others, 2006; Iverson, this volume, chap. 21). Models from GPS (Lisowski and others, this volume, chap. 15) and InSAR data (Poland and Lu, this volume, chap. 18) yield estimates of reservoir volume loss of $15–30\times10^6$ m^3, compared with a volume of $70–80\times10^6$ m^3 for the lava dome. This disparity most likely reflects a combination of expansion of magmatic volatiles and recharge (Mastin and others, this volume, chap. 22). However, erupted volumes and total volatile output for the 2004–5 eruption were used to estimate the volatile content of magma at 8.6-km depth. Gerlach and others (this volume, chap. 26) conclude that the magma was nearly depleted in excess volatiles, suggesting that new gas-rich magma has not been added into the reservoir during the months just before or during the eruption.

Volume measurements of the growing lava dome and derived extrusion rates help to place the 2004–5 eruption in context with those of other dome-building volcanoes (fig. 10) and within the growth history of Mount St. Helens since 1980. The average rate of growth of the current dome, about 2 m^3/s through the end of 2005, is an order of magnitude above the long-term (1980–present) eruption rate of Mount St. Helens (Iverson, this volume, chap. 21). However, when compared to other dome-growth episodes at Mount St. Helens and elsewhere the current growth rate is fairly typical (fig. 10).

Conclusions

Vertical aerial photographs, taken at time intervals ranging from successive days to every few weeks, and the digital elevation models (DEMs) constructed from them have been critical tools to document the remarkable growth history of the 2004–5 lava dome at Mount St. Helens, especially in providing estimates of volume and volumetric extrusion rate. Single DEMs provided length and width measurements of the dome and glacier; sequential DEMs recorded temporal and spatial changes. Moreover, measurements of volume and volumetric extrusion rate proved to be critical parameters. When combined with other primary data sets, they helped to form models and hypotheses that illuminated the mechanics and dynamics of the eruption, and thus helped to assess volcano hazards. The successful application of aerophotogrammetry to monitor this eruption was possible largely because baseline data and photogrammetric infrastructure were in place before the onset of activity. The aerial photos and DEMs obtained in this study are an enduring resource for addressing basic questions about the eruption, including many raised in other papers in this collection and, we suspect, others yet to be asked.

Acknowledgments

We thank Richard Iverson, Richard Herd, and Dan Dzurisin for their insightful and helpful reviews. Dan Dzuri-

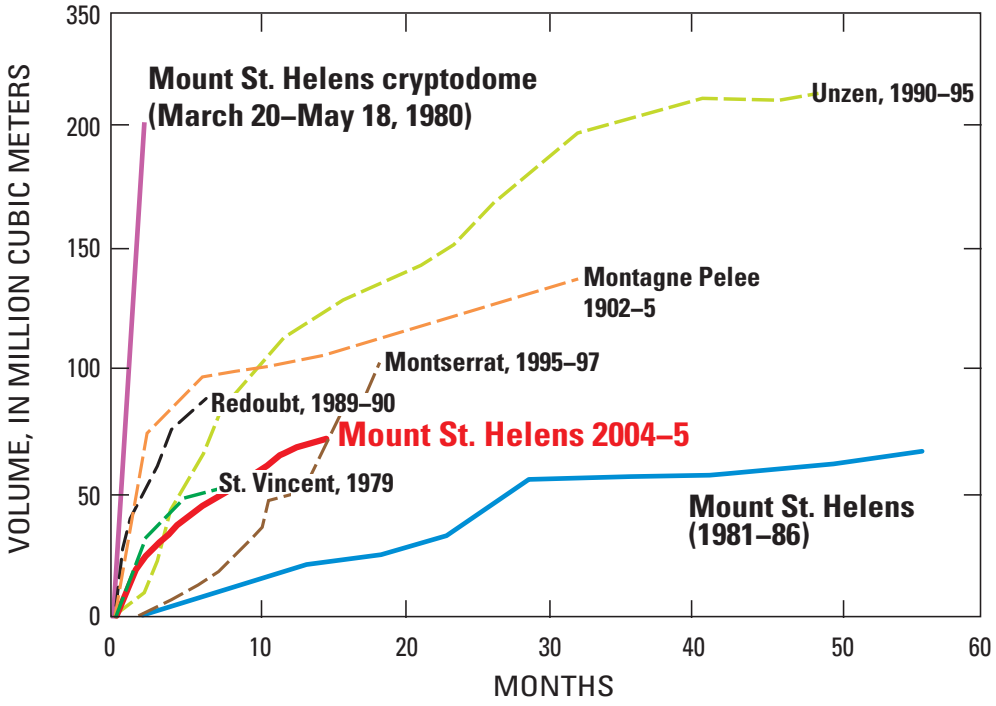

Figure 10. Mount St. Helens 2004–2005 growth rate curve compared with other historical lava domes (modified from Nakada and others, 1999; Tanguy, 2004).

sin also contributed insightful and helpful discussions. Bergman Photographic Services, including Larry and Bruce Bergman, Travis Marshall, Trevor Gray, Steve Tank, Kyla Dorsey, and John Hogl, have all contributed their expertise to ensure that we acquired excellent aerial photographs and scans. We are indebted to Jeff Linscott and the folks at JL Aviation for outstanding helicopter work, especially landing us gently in difficult places on the mountain for ground control work. Frank Trusdell, Mike Poland, Julie Griswold, Chris Harpel, Dave Ramsey, Joel Robinson, Stephanie Konfal, Angie Diefenbach, Sarah Thompson, and Susanne Ettinger helped with ground control work and offered insightful discussions. Last, but perhaps most important, we thank Bobbie Myers, who watched over us remotely, tracked our safety, and allowed us to focus on field tasks.

References Cited

Achilli, V., Baldi, P., Baratin, L., Bonini, C., Ercolani, E., Gandolfi, S., Anzidei, M., and Riguzzi, F., 1998, Digital photogrammetric survey on the island of Vulcano: Acta Vulcanologica, v. 10, no. 1, p. 1–5.

Baldi, P., Bonvalot, S., Briole, P., and Marsella, M., 2000, Digital photogrammetry and kinematic GPS applied to the monitoring of Vulcano Island, Aeolian arc, Italy: Geophysics Journal International, v. 142, no. 3, p. 801–811.

Baldi, P., Fabris, M., Marsella, M., and Monticelli, R., 2005, Monitoring the morphological evolution of the Sciara del Fuoco during the 2002–2003 Stromboli eruption using multi-temporal photogrammetry: ISPRS Journal of Photogrammetry and Remote Sensing, v. 59, no. 4, p. 199–211.

Daniel, C., and Tennant, K., 2001, DEM quality assessment, *in* Maune, D., ed., Digital elevation model technologies and applications; the DEM users manual: Town, Maryland, American Society of Photogrammetry and Remote Sensing, 539 p.

Dzurisin, D., 2003, A comprehensive approach to monitoring volcano deformation as a window on the eruption cycle: Reviews of Geophysics, v. 41, no. 1, 29 p., doi:10.1029/2001RG000107.

Dzurisin, D., Vallance, J.W., Gerlach, T.M., Moran, S.C., and Malone, S.D., 2005, Mount St. Helens reawakens: Eos (American Geophysical Union Transactions), v. 86, no. 3, p. 25, 29.

Dzurisin, D., Lisowski, M., Poland, M.P., Sherrod, D.R., and LaHusen, R.G., 2008, Constraints and conundrums resulting from ground-deformation measurements made during the 2004–2005 dome-building eruption of Mount St. Helens, Washington, chap. 14 *of* Sherrod, D.R., Scott, W.E., and Stauffer, P.H., eds., A volcano rekindled; the renewed eruption of Mount St. Helens, 2004–2006: U.S. Geological Survey Professional Paper 1750 (this volume).

Gerlach, T.M., McGee, K.A., and Doukas, M.P., 2008, Emission rates of CO_2, SO_2, and H_2S, scrubbing, and preeruption excess volatiles at Mount St. Helens, 2004–2005, chap. 26 *of* Sherrod, D.R., Scott, W.E., and Stauffer, P.H., eds., A volcano rekindled; the renewed eruption of Mount St. Helens, 2004–2006: U.S. Geological Survey Professional Paper 1750 (this volume).

Harris, A.J.L., Rose, W.I., and Flynn, L.P., 2003, Temporal trends in lava dome extrusion at Santiaguito 1922–2000: Bulletin of Volcanology, v. 65, p. 77–89.

Herriott, T.M., Sherrod, D.R., Pallister, J.S., and Vallance, J.W., 2008, Photogeologic maps of the 2004–2005 Mount St. Helens eruption, chap. 10 *of* Sherrod, D.R., Scott, W.E., and Stauffer, P.H., eds., A volcano rekindled; the renewed eruption of Mount St. Helens, 2004–2006: U.S. Geological Survey Professional Paper 1750 (this volume).

Iverson, R.M., 2008, Dynamics of seismogenic volcanic extrusion resisted by a solid surface plug, Mount St. Helens, 2004–2005, chap. 21 *of* Sherrod, D.R., Scott, W.E., and Stauffer, P.H., eds., A volcano rekindled; the renewed eruption of Mount St. Helens, 2004–2006: U.S. Geological Survey Professional Paper 1750 (this volume).

Iverson, R.M., Dzurisin, D., Gardner, C.A., Gerlach, T.M., LaHusen, R.G., Lisowski, M., Major, J.J., Malone, S.D., Messerich, J.A., Moran, S.C., Pallister, J.S., Qamar, A.I., Schilling, S.P., and Vallance, J.W., 2006, Dynamics of seismogenic volcanic extrusion at Mount St. Helens in 2004–2005: Nature, v. 444, no. 7118, p. 439–443, doi:10.1038/nature05322.

Lescinsky, D.T., and Fink, J.H., 2000, Lava and ice interaction at stratovolcanoes; use of characteristic features to determine past glacial extents and future volcanic hazards: Journal of Geophysical Research, v. 105, no. B10, p. 23711–23726.

Lisowski, M., Dzurisin, D., Denlinger, R.P., and Iwatsubo, E.Y., 2008, Analysis of GPS-measured deformation associated with the 2004–2006 dome-building eruption of Mount St. Helens, Washington, chap. 15 *of* Sherrod, D.R., Scott, W.E., and Stauffer, P.H., eds., A volcano rekindled; the renewed eruption of Mount St. Helens, 2004–2006: U.S. Geological Survey Professional Paper 1750 (this volume).

Major, J.J., Kingsbury, C.G., Poland, M.P., and LaHusen, R.G., 2008, Extrusion rate of the Mount St. Helens lava dome estimated from terrestrial imagery, November 2004–December 2005, chap. 12 *of* Sherrod, D.R., Scott, W.E., and Stauffer, P.H., eds., A volcano rekindled; the renewed eruption of Mount St. Helens, 2004–2006: U.S. Geological Survey Professional Paper 1750 (this volume).

Mastin, L.G., Roeloffs, E., Beeler, N.M., and Quick, J.E., 2008, Constraints on the size, overpressure, and volatile content of the Mount St. Helens magma system from geodetic and dome-growth measurements during the 2004–2006+ eruption, chap. 22 *of* Sherrod, D.R., Scott, W.E., and Stauffer, P.H., eds., A volcano rekindled; the renewed eruption of Mount St. Helens, 2004–2006: U.S. Geological Survey Professional Paper 1750 (this volume).

Messerich, J.A., Schilling, S.P., and Thompson, R.A., 2008, Digital elevation models of the pre-eruption 2000 crater and 2004–07 dome-building eruption at Mount St. Helens, Washington, U.S.A.: U.S. Geological Survey Open-File Report 2008–1169, 2 p., with digital database. [http://pubs.usgs.gov/of/2008/1169, last accessed July 15, 2008].

Miller, T.P., 1994, Dome growth and destruction during the 1989–1990 eruption of Redoubt Volcano: Journal of Volcanology and Geothermal Research, v. 62, nos. 1–4, p. 197–212.

Mills, H.H., 1992, Post-eruption erosion and deposition in the 1980 crater of Mount St. Helens, Washington, determined from digital maps: Earth Surface Processes and Landforms, v. 17, no. 8, p. 739–754.

Moore, J.G., and Albee, W.C., 1981, Topographic and structural changes, March–July 1980—photogrammetric data, *in* Lipman, P.W., and Mullineaux, D.R., eds,, The 1980 eruptions of Mount St. Helens, Washington: U.S. Geological Survey Professional Paper 1250, p. 123–134.

Moran, S.C., Malone, S.D., Qamar, A.I., Thelen, W.A., Wright, A.K., and Caplan-Auerbach, J., 2008, Seismicity associated with renewed dome building at Mount St. Helens, 2004–2005, chap. 2 *of* Sherrod, D.R., Scott, W.E., and Stauffer, P.H., eds., A volcano rekindled; the renewed eruption of Mount St. Helens, 2004–2006: U.S. Geological Survey Professional Paper 1750 (this volume).

Nakada, S., Shimizu, H., and Ohta, K., 1999, Overview of the 1990–1995 eruption at Unzen Volcano: Journal of Volcanology and Geothermal Research, v. 89, nos. 1–4, p. 1–22, doi:10.1016/S0377-0273(98)00118-8.

Newhall, C.G., and Melson, W.G., 1983, Explosive activity associated with the growth of volcanic domes: Journal of Volcanology and Geothermal Research, v. 17, p. 111–131.

Pallister, J.S., Thornber, C.R., Cashman, K.V., Clynne, M.A., Lowers, H.A., Mandeville, C.W., Brownfield, I.K., and Meeker, G.P., 2008, Petrology of the 2004–2006 Mount St. Helens lava dome—implications for magmatic plumbing and eruption triggering, chap. 30 *of* Sherrod, D.R., Scott, W.E., and Stauffer, P.H., eds., A volcano rekindled; the renewed eruption of Mount St. Helens, 2004–2006: U.S. Geological Survey Professional Paper 1750 (this volume).

Poland, M.P., and Lu, Z., 2008, Radar interferometry observations of surface displacements during pre- and coeruptive periods at Mount St. Helens, Washington, 1992–2005, chap. 18 *of* Sherrod, D.R., Scott, W.E., and Stauffer, P.H., eds., A volcano rekindled; the renewed eruption of Mount St. Helens, 2004–2006: U.S. Geological Survey Professional Paper 1750 (this volume).

Queija, V.R., Stoker, J.M., and Kosovich, J.J., 2005, Recent U.S. Geological Survey applications of Lidar: Photogrammetric Engineering and Remote Sensing, v. 71, no. 1, p. 5–9.

Schilling, S.P., Carrara, P.E., Thompson, R.A., and Iwatsubo, E.Y., 2004, Posteruption glacier development within the crater of Mount St. Helens, Washington, USA: Quaternary Research, v. 61, p. 325–329.

Sparks, R.S.J., Young, S.R., Barclay, J., Calder, E.S., Cole, P., Darroux, B., Davies, M.A., Druitt, T.H., Harford, C., Herd, R., James, M., Lejeune, A.M., Norton, G., Skerrit, G., Stasiuk, M.V., Stevens, N.S., Toothill, J., Wadge, G., and Watts, R., 1998, Magma production and growth of the lava dome of the Soufriere Hills Volcano, Montserrat, West Indies; November 1995 to December 1997: Geophysical Research Letters, v. 25, no. 18, p. 3421–3424.

Swanson, D.A., and Holcomb, R.T., 1990, Regularities in growth of the Mount St. Helens dacite dome, 1980–1986, *in* Fink, J.H., ed., Lava flows and domes, emplacement mechanisms and hazard implications: Berlin, Springer-Verlag, International Association of Volcanology and Chemistry of the Earth's Interior, Proceedings in Volcanology 2, p. 3–24.

Swanson, D.A., Lipman, P.W., Moore, J.G., Heliker, C.C., and Yamashita, K.M., 1981, Geodetic monitoring after the May 18 eruption, *in* Lipman, P.W., and Mullineaux, D.R., eds., The 1980 eruptions of Mount St. Helens, Washington: U.S. Geological Survey Professional Paper 1250, p. 157–168.

Tanguy, J.-C., 2004, Rapid dome growth at Montagne Pelée during the early stages of the 1902–1905 eruption; a reconstruction from Lacroix's data: Bulletin of Volcanology, v. 66, no. 7, p. 615–621, doi:10.1007/s00445-004-0344-z.

Thompson, R.A., and Schilling, S.P., 2007, Photogrammetry, *in* Dzurisin, D., ed., Volcano deformation—geodetic monitoring techniques: Berlin, Springer, Springer-Praxis Books in Geophysical Sciences, p. 195–221.

Vallance, J.W., Schneider, D.J., and Schilling, S.P., 2008, Growth of the 2004–2006 lava-dome complex at Mount St. Helens, Washington, chap. 9 *of* Sherrod, D.R., Scott, W.E., and Stauffer, P.H., eds., A volcano rekindled; the renewed eruption of Mount St. Helens, 2004–2006: U.S. Geological Survey Professional Paper 1750 (this volume).

Walder, J.S., Schilling, S.P., Vallance, J.W., and LaHusen, R.G., 2008, Effects of lava-dome growth on the Crater Glacier of Mount St. Helens, Washington, chap. 13 *of* Sherrod, D.R., Scott, W.E., and Stauffer, P.H., eds., A volcano

rekindled; the renewed eruption of Mount St. Helens, 2004–2006: U.S. Geological Survey Professional Paper 1750 (this volume).

Wolf, P.R., and Dewitt, B.A., 2000, Elements of photogrammetry with applications in GIS (3d ed.): Boston, McGraw-Hill, 608 p.

Zilkoski, D.B., Richards, J.H., and Young, G.M., 1992, Special report—results of the general adjustment of the North American Vertical Datum of 1988: Surveying and Land Information Systems, v. 52, p. 133–149.

Zlotnicki, J., Ruegg, J.C., Bachelery, P., and Blum, P.A., 1990, Eruptive mechanism on Piton de la Fournaise volcano associated with the December 4, 1983, and January 18, 1984 eruptions from ground deformation monitoring and photogrammetric surveys: Journal of Volcanology and Geothermal Research, v. 40, no. 3, p. 197–217, doi:10.1016/0377-0273(90)90121-U.

Appendix 1. Hillslope Shaded-Relief Maps

[This appendix appears only in the digital versions of this work—in the DVD that accompanies the printed volume and as a separate file accompanying this chapter on the Web at: http://pubs.usgs.gov/pp/1750.]

The appendix contains 17 raster images in Tagged Image File Format (filename extension is “tif”), one for each of the hillshade relief maps used in figures 4, 6, 7, and 8. The filename contains the date (year-month-day) of the map. Corresponding ASCII world files (filename extension “tfw”) for georeferencing the raster maps by GIS software are included, each using the Universal Transverse Mercator projection, zone 10, North American Datum 1983. A separate metadata file summarizes the pertinent details of image processing.